MOX-Report No. 37/2015

Educated bases for the HiMod reduction of advection-diffusion-reaction problems with general boundary conditions

Aletti, M.; Perotto, S.; Veneziani, A.

Educated bases for the HiMod reduction of advection-diffusion-reaction problems with general boundary conditions

Matteo Aletti[♭],[∗] Simona Perotto[♭] and Alessandro Veneziani[♯]

June 29, 2015

[♭] MOX– Modellistica e Calcolo Scientifico
Dipartimento di Matematica, Politecnico di Milano
Piazza Leonardo da Vinci 32, 20133 Milano, Italy
`matteo.aletti@mail.polimi.it`, `simona.perotto@polimi.it`
[♯] Department of Mathematics and Computer Science, Emory University
400 Dowman Dr NE, S.te N416, Atlanta GA, USA 30322
`ale@mathcs.emory.edu`

Keywords: model reduction; spectral/finite element combined approximation, Robin boundary conditions, Sturm-Liouville eigenvalue problem

AMS Subject Classification: 65N30, 65N35, 76M10, 76M22, 78M34

Abstract

Hierarchical Model (HiMod) reduction is a method introduced in [1] to effectively solve advection-diffusion-reaction (ADR) and fluid dynamics problems in pipes. The rationale of the method is to regard the solution as a mainstream axial dynamics added by transverse components. The mainstream component is approximated by finite elements as often done in classical 1D models (like the popular Euler equations for gasdynamics). However, the HiMod formulation includes also the transverse dynamics by a spectral expansion. A few modes are expected to capture the transverse (somehow secondary) dynamics with a good level of approximation. This drastically reduces the size of the discrete problem, yet preserving accuracy. The method is "hierarchical" since the selection of the number of transverse modes can be hierarchically and adaptively performed [12]. We have previously considered only Dirichlet boundary conditions for the lateral walls of the pipe and the procedure was tested only in 2D domains. With an appropriate selection

---

[∗]Current affiliation: Inria Paris-Rocquencourt & Sorbonne Universités UPMC Univ Paris 6, Laboratoire Jacques-Louis Lions, France.

1

of the spectral basis functions, here we extend our formulation to 3D problems with general boundary conditions, still pursuing an essential approach. The modal basis functions fulfill by construction the (homogeneous) boundary conditions associated with the solution. This is achieved by solving a Sturm-Liouville eigenpair problem. We analyze this approach and provide a convergence analysis for the numerical error in the case of a linear ADR problem in rectangles (2D) and slabs (3D). Numerical results confirm the theory.

1   Introduction

Efficient numerical solution of problems characterized by a main direction like flow in pipes and networks has been investigated in several ways, as witnessed by engineering and mathematical literature (see, e.g., [2, 3, 4]). A popular approach is based on the reduction of the problem of interest to a one dimensional setting along the mainstream after dropping transversal dynamics. The Euler equations in gas- and haemo-dynamics are a well known example. A numerical approach aiming at reducing the computational cost vs a full 3D simulation without discarding the transversal dynamics has been proposed in [1, 7] and investigated in [6, 20, 12]. Since the axial direction is expected to drive the solution while transverse dynamics is only locally important, it makes sense to split the approximation of the two components. Along the mainstream we consider a classical 1D finite element approximation to exploit easiness and versatility of this method. The transversal components are tackled by a spectral approximation. The rationale is that the high convergence rate of spectral approximations allow to capture the important features of the transverse dynamics with a relatively low number of modes. This results in accurate approximations with a low number of degrees of freedom.

The splitting of axial and transverse directions has been considered for combining different spectral approximation methods in different contexts. For instance, see [13, 14, 15, 16, 17, 23], Sect. 3.4 of [10] and references therein. The number of modes can be properly selected either with an a priori but not necessarily uniform approach[1, 7] or adaptively with either a domain splitting [12] or a nodewise perspective[5]. Even though most of the theory has been developed on rectilinear domains, extension to curved domains is a natural and important follow-up[6]. This approach was intended to improve the reliability of one dimensional models. As opposed to purely 1D models, this approach allows in fact a local refinement of the reliability by properly selecting the number m of modes, in what has been called a "psychologically 1D" modeling strategy. For this reason the approach has been called *Hierarchical Model* (HiMod) reduction.

One of the most significant limitations of the approach pursued so far is the conditions to be prescribed on the lateral boundary of the domain. As a matter of fact, homogeneous Dirichlet conditions were promptly included by the sinusoidal basis functions adopted for this problem. Although, these conditions describe many practical applications, in view of generalizations of the HiMod approach to more

complex problems such as fluid-structure interaction (for instance in arteries), we need to address more general boundary conditions.

In this paper we present a method for this. The method follows a classical approach by solving an associated Sturm-Liouville Eigenvalue (SLE) problem. In this way the basis functions include the information on the boundary conditions, so we call this an "educated" basis function approach (Sect. 3).

We introduce the methodology in either 2D rectangular domains or 3D slabs, together with the analysis of the associated numerical error in Sect. 4.

Numerical results confirming theoretical findings are presented both in 2D and 3D (Sect. 5) domains for linear advection-diffusion-reaction problems. A backward facing step geometry is used as a nontrivial slab-like domain.

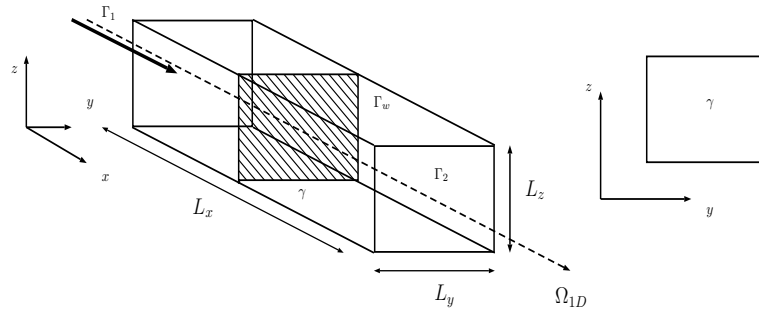Limitations and future developments are summarized in Sect. 6

Figure 1: 3D domain setting for the HiMod educated bases approach: domain $\Omega \equiv \widehat{\Omega}$ (left) and transverse fiber γ (right).

2 The HiMod approach: basics

Since in this paper we are concerned with rectangular/slab domains, we directly assume that $\Omega \subset \mathbb{R}^d$ ($d = 2, 3$) coincides with the Cartesian product of a 1D domain supporting the axis Ω_{1D} and transverse fibers $\gamma_x \subset \mathbb{R}^{d-1}$, i.e.,

$$\Omega = \bigcup_{x \in \Omega_{1D}} \{x\} \times \gamma_x$$

(see Fig. 1). The axial direction associated with Ω_{1D} is dominant with respect to the others (i.e. $L_x \gg L_y, L_z$). Hereafter, we choose $\Omega_{1D} \equiv (0, L)$ and $\gamma_x = \gamma \equiv (0, 1)$ for the 2D case, $\gamma_x = \gamma \equiv (0, 1) \times (0, 1)$ in 3D. More in general, we may assume that Ω_{1D} is a curve $\mathcal{C} : (0, L) \to \Omega_{1D} \subset \mathbb{R}^2$, where x is a curvilinear abscissa[6], while fibers γ_x coincide with sufficiently regular functions of x. In this case, we regard Ω as the image of the reference rectangular/slab domain $\widehat{\Omega} = [0, L] \times \gamma$, according to a sufficiently regular map[1, 7].

In Ω we solve the standard scalar linear advection-diffusion-reaction (ADR) problem completed - for the moment being - with full homogeneous Dirichlet

3

boundary conditions. With standard notation for the Sobolev spaces[19], the problem reads: find $u \in V \equiv H_0^1(\Omega)$ such that

$$a(u, v) = \int_\Omega \left[\mu \nabla u \cdot \nabla v + (\boldsymbol{\beta} \cdot \nabla u + \sigma u)v \right] d\Omega = \int_\Omega f v \, d\Omega = F(v) \quad \forall v \in V, \quad (1)$$

where the boundary $\partial \Omega$ consists of the two transverse fibers $\Gamma_1 = \{0\} \times \gamma$ and $\Gamma_2 = \{L\} \times \gamma$ and of the lateral boundary $\Gamma_w \equiv \partial \Omega \setminus \{\Gamma_1 \cup \Gamma_2\}$ (see Fig. 1). We assume the diffusivity coefficient $\mu \in L^\infty(\Omega)$, with $\mu \geq \mu_0 > 0$ a.e. in Ω, the convective field $\boldsymbol{\beta} \in [L^\infty(\Omega)]^d$, the reactive coefficient $\sigma \in L^\infty(\Omega)$, and the forcing term $f \in L^2(\Omega)$. We also assume that $\mathrm{div}(\boldsymbol{\beta}) \in L^\infty(\Omega)$ and that $-\frac{1}{2}\mathrm{div}(\boldsymbol{\beta}) + \sigma > 0$ a.e. in Ω, so that the well-posedness of (1) follows from the Lax-Milgram lemma.

The HiMod formulation requires a specific functional setting. We introduce the one-dimensional space $V_{1D} \equiv H_0^1(\Omega_{1D})$ associated with the supporting fiber. On the transverse direction we consider a set of modal functions $\{\varphi_k\}$ with $k \in \mathbb{N}^+$, defined on γ and set $V_{\gamma,\infty} = \mathrm{span}(\{\varphi_k\})$. Since the Dirichlet conditions are enforced in an essential way, basis functions φ_k vanish on Γ_w. The corresponding truncated finite dimensional space $V_{\gamma,m}$ is defined as

$$V_{\gamma,m} = \mathrm{span}(\{\varphi_k\}_{k=1}^m). \quad (2)$$

Thus, the hierarchically reduced semi-discrete space associated with Ω is given by the tensor product of the spaces V_{1D} and $V_{\gamma,m}$, i.e., by

$$V_m = V_{1D} \otimes V_{\gamma,m} = \left\{ v(x, \mathbf{y}) = \sum_{k=1}^m v_k(x)\varphi_k(\mathbf{y}), \text{ with } v_k \in V_{1D} \text{ for } k = 1 \ldots m \right\}. \quad (3)$$

We assume that $V_m \subset V$ for any $m \in \mathbb{N}$ (*conformity hypothesis*), and that, for any $v \in V$,

$$\lim_{m \to +\infty} \left(\inf_{v_m \in V_m} ||v - v_m||_V \right) = 0 \quad \textit{(spectral approximability hypothesis)} .$$

When we let m tend to infinity, we identify the space V_∞. The conformity and spectral approximability properties postulated on V_m imply that V_∞ is dense in $H_0^1(\Omega)$.

The basis functions φ_k do not need to be generally orthonormal. However, if we assume they are orthonormal with respect to the $L^2(\gamma)$-scalar product $(\cdot, \cdot)_\gamma$, the coefficients v_k in (3) coincide with the standard Fourier coefficients

$$v_k = (v, \varphi_k)_\gamma. \quad (4)$$

Different choices are possible for the modal basis, including trigonometric functions, Legendre polynomials or wavelets. The problem at hand generally drives this choice.

The fully-discrete HiMod formulation can be provided by introducing a uniform subdivision $\mathcal{T}_h$ of step h along Ω_{1D}, with the nodes x_i, $i = 0, 1, \ldots, N_h$. In [12] a HiMod reduction based on an adaptive choice of the partition $\mathcal{T}_h$ is presented. We denote by V^h the subspace of V_{1D} of the piecewise continuous linear functions associated with $\mathcal{T}_h$ and vanishing at $x_0 = 0$ and $x_{N_h} = L$. Higher degree polynomials may be considered as well. Let ψ_i denote the Lagrangian basis function in V^h associated with the node x_i. Thus, we can consider the discrete modal representation

$$u_m^h(x, \mathbf{y}) = \sum_{k=1}^{m} u_k(x)\varphi_k(\mathbf{y}) = \sum_{k=1}^{m}\sum_{i=1}^{N_h} u_{k,i}\psi_i(x)\varphi_k(\mathbf{y}), \tag{5}$$

where $u_{k,i}$ are the actual unknowns of the discrete HiMod formulation

$$\text{find } u_m^h \in V_m^h : a(u_m^h, v_m^h) = F(v_m^h) \quad \forall v_m^h \in V_m^h, \tag{6}$$

with $u_k(x) = \sum_{1=1}^{N_h} u_{k,i}\psi_i(x) \in V_h$, and where $V_m^h = V^h \otimes V_{\gamma,m}$. A straightforward choice for the test function in (6) is $v_m^h(x, \mathbf{y}) = \psi_l(x)\varphi_j(\mathbf{y})$, with $l = 1, \ldots, N_h$, $j = 1, \ldots, m$. Then, the HiMod formulation (6) reduces to: find $u_{k,i} \in \mathbb{R}^{mN_h}$ such that, for any $j = 1, \ldots, m$ and for any $l = 1, \ldots, N_h$,

$$\sum_{k=1}^{m}\sum_{i=1}^{N_h}\Bigg\{\int_{\Omega_{1D}}\Bigg[\quad r_{k,j}^{11}(x)\frac{\partial\psi_i}{\partial x}(x)\frac{\partial\psi_l}{\partial x}(x) + r_{k,j}^{10}(x)\frac{\partial\psi_i}{\partial x}(x)\psi_l(x)$$

$$+ \quad r_{k,j}^{00}\psi_i(x)\psi_l(x)\Bigg]\,dx\Bigg\}u_{k,i} = \int_{\Omega_{1D}}\psi_l(x)f_j(x)\,dx, \quad (7)$$

with

$$r_{k,j}^{11}(x) = \int_{\gamma}\mu(x,\mathbf{y})\varphi_j(\mathbf{y})\varphi_k(\mathbf{y})\,d\mathbf{y}, \quad r_{k,j}^{10}(x) = \int_{\gamma}\beta_1(x,\mathbf{y})\varphi_j(\mathbf{y})\varphi_k(\mathbf{y})\,d\mathbf{y},$$

$$r_{k,j}^{00}(x) = \int_{\gamma}\Big(\mu(x,\mathbf{y})\varphi_j'(\mathbf{y})\varphi_k'(\mathbf{y}) + \beta_2(x,\mathbf{y})\varphi_j'(\mathbf{y})\varphi_k(\mathbf{y}) + \sigma(x,\mathbf{y})\varphi_j(\mathbf{y})\varphi_k(\mathbf{y})\Big)d\mathbf{y},$$

$$f_j(x) = \int_{\gamma}f(x,\mathbf{y})\varphi_j(\mathbf{y})\,d\mathbf{y},$$

$$\tag{8}$$

where $\varphi_l'(\mathbf{y})$ denotes the derivative of the generic modal function φ_l with respect to $\mathbf{y}$. Coefficients $r_{k,j}^{st}$ ($s, t = 0, 1$) collect the transverse contributions after the reduction phase. If the modal basis is orthogonal the computation of these coefficients is further simplified. On the contrary, definitions (8) become significantly more involved for non-rectangular domains[1].

Discretization (7) leads to an algebraic system of m coupled 1D problems, where the coefficients coupling the different 1D equations account for the transverse dynamics. The HiMod discrete solution u_m^h converges to the continuous one u for $m \to +\infty$ and $h \to 0$, as stated in Proposition 3.1 of [7].

Remark 2.1 *Non-homogeneous boundary conditions of Dirichlet, Neumann and Robin type are promptly prescribed on the inflow/outflow boundaries Γ_1 and Γ_2 in the HiMod framework with standard methods[7].*

2.1 Dirichlet problems in 3D

In this section, we demonstrate for the first time some performances of the HiMod method in 3D. This allows to stress how a good accuracy may be obtained with a relatively low number of degrees of freedom. This is crucial for the prospected application of the method on complex networks.

Let us consider the following advection-diffusion-reaction problem in a slab

$$\begin{cases} -\Delta u + \boldsymbol{\beta} \cdot \nabla u + \sigma u = f & \text{in } \Omega = (0, 0.2) \times (0, 0.1) \times (0, 0.1) \\ u = 0 & \text{on } \Gamma_1 \cup \Gamma_w \\ \nabla u \cdot \boldsymbol{n} = 0 & \text{on } \Gamma_2, \end{cases} \tag{9}$$

with $\Gamma_1 = \{0\} \times [0, 0.1] \times [0, 0.1]$, $\Gamma_2 = \{0.2\} \times [0, 0.1] \times [0, 0.1]$ and $\Gamma_w = \partial\Omega \setminus (\Gamma_1 \cup \Gamma_2)$, and where $\boldsymbol{\beta} = (5, 1, 0)^T$ is a horizontal wind, $\sigma = 0.3$ models an absorption phenomenon, and f is a source term localized in correspondence with two spheric areas of Ω defined by $f(x, y, z) = 100\big(f_1(x, y, z) + f_2(x, y, z)\big)$, with $f_1(x, y, z) = \exp\big(-900\big[(x - 0.025)^2 + (y - 0.0125)^2 + (z - 0.0125)^2\big]\big)$, $f_2(x, y, z) = \exp\big(-900\big[(x-0.05)^2 + (y-0.0875)^2 + (z-0.0875)^2\big]\big)$. Figure 2, left shows the contour surfaces of the finite element approximation of the solution computed via the library $\texttt{LifeV}$[1] on a structured uniform mesh with sizes $h_x = 0.1$, $h_y = 0.05$, $h_z = 0.05$, respectively. The HiMod approximation is obtained using 50 modal functions and a 1D uniform grid with step $h_x = 0.1$ (Fig. 2, right).
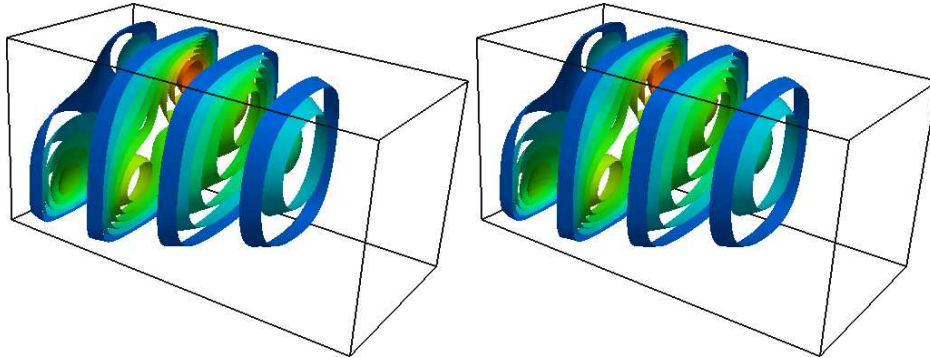

Figure 2: 3D ADR problem with wall Dirichlet boundary conditions: Piecewise linear FE solution (left); HiMod solution (right).

---

[1]$\texttt{LifeV}$ is an open source finite element library developed by MOX at Politecnico di Milano, Italy, the Department of Mathematics at EPFL, Switzerland and the Department of Mathematics and Computer Science at Emory University, USA.
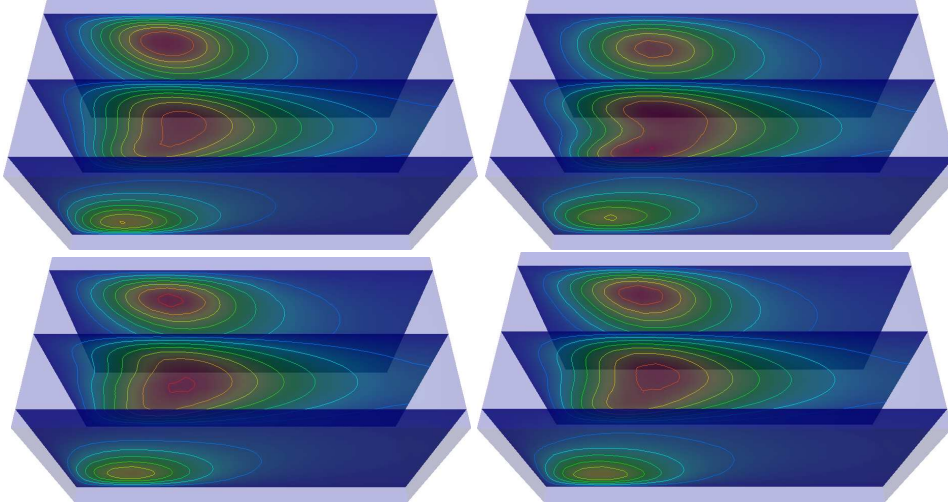
Figure 3: 3D ADR problem: longitudinal sections of the FE solution (top-left) and of the HiMod solutions for $m = 9$ (top-right), $m = 16$ (bottom-left) and $m = 25$ (bottom-right).

The consistency between the two solution is promptly realized by a visual inspection. In Figure 3 we consider three longitudinal sections of both the reference and the HiMod solution at $y = 0.1$, 0.05, 0.09 respectively. We select increasing values for the modal index m, namely, $m = 9$, $m = 16$ and $m = 25$. More precisely, this choice of m corresponds to 3, 4 and 5 modes along the two transverse directions, respectively. We appreciate the qualitative convergence of the HiMod solution to the finite element one for increasing values of m.

To make the comparison more quantitative, we solve the same equation with $\boldsymbol{\beta} = (5, 1, 1)^T$, $\sigma = 3$ and we select the source term and the Dirichlet condition on Γ_1 so that the exact solution is $u_{ex}(x, y, z) = 10^7 y(0.1 - y)z(0.1 - z)(x - 0.2)^2 \exp(2yz(0.2 - x)^2)$. In Fig. 4 we plot the $L^2(\Omega)$-norm of the global error, as a function of the total number of the degrees of freedom (dof) on the left, and as a function of the assembly time (in LifeV) on the right.

As expected for the convergence properties of the spectral transverse approximation, the HiMod procedure attains a similar accuracy of finite elements (or better) with less dof. Precisely, the structured FE grid features $N_x N_y N_z$ dof, where N_x, N_y and N_z are the numbers of dof along the three directions. For HiMod we have $N_x m$ dof, so for $m \ll N_y N_z$ we have a computational advantage.

These results confirm the rationale of the HiMod approach, where a few modes are enough to have an accurate solution as opposed to purely 1D approximations, where transverse dynamics are completely discarded.
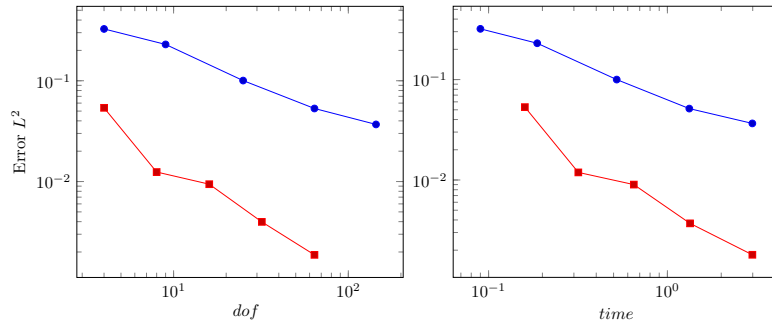
Figure 4: 3D ADR problem with lateral Dirichlet boundary conditions: $L^2(\Omega)$-norm of the global error as a function of the number of dof (left) and of the assembly time[s] (right) for a standard 3D linear finite element discretization (circle markers) and for a HiMod approximation (square markers).

3 The Sturm-Liouville Eigenvalue (SLE) problem in the HiMod framework

In order to construct a set of basis functions incorporating general (homogeneous) boundary conditions on Γ_w, we consider the classical SLE problem[8]. We consequently focus on the transverse fiber $\gamma \subset \mathbb{R}^{d-1}$. In particular, we are interested in the cases $d = 2, 3$, where we have 1D and 2D fibers respectively. We recall here some basic results that can be found for instance in [8, 9]. We write down the proofs of the results that generalize to the case $d = 3$ of the ones found there.

3.1 Spectrum of a self-adjoint elliptic operator

Let $\mathcal{L}_s$ be a linear elliptic symmetric operator defined over the regular bounded domain γ. Then, we consider the eigenvalue problem

$$\mathcal{L}_s \varphi_k(\mathbf{y}) = \lambda_k w(\mathbf{y}) \varphi_k(\mathbf{y}), \tag{10}$$

where λ_k is the eigenvalue of $\mathcal{L}_s$ associated with the eigenfunction φ_k, while the weight w is a positive continuous function. The following statements hold.

1. The eigenvalues $\{\lambda_k\}$ are real and form a countable monotone non-decreasing sequence convergent to infinity for $k \to +\infty$. In the one-dimensional case (i.e., for $d = 2$), the multiplicity of all the eigenvalues is equal to one.

2. The eigenfunctions $\{\varphi_k\}$ are orthogonal with respect to the $L_w^2(\gamma)$-weighted scalar product. They constitute a complete set in the same space. This means that, for a generic function $f \in L_w^2(\gamma)$, the truncated series

$$\mathcal{S}_m f(\mathbf{y}) = \sum_{k=1}^{m} \hat{f}_k \varphi_k(\mathbf{y}), \tag{11}$$

8

with $\hat{f}_k = \int_\gamma w(\mathbf{y})f(\mathbf{y})\varphi_k(\mathbf{y})\,d\mathbf{y}$, is such that

$$\lim_{m \to +\infty} \|f - \mathcal{S}_m f\|_w = 0, \tag{12}$$

where $\|\cdot\|_\omega$ denotes the norm associated with the space $L_w^2(\gamma)$. From now on, we refer to the basis functions $\{\varphi_k\}$ in (10) guaranteeing expansion (11) as to the SL basis.

3. For $k \to +\infty$, the asymptotic Weyl formula for the eigenvalues in (10) holds[25, 8]:

$$\lambda_k = \mathcal{O}\left(k^{\frac{2}{d-1}}\right). \tag{13}$$

For the derivation of a one-dimensional ($d = 2$) HiMod educated basis, we focus on the following SLE problem: for $y \in (0,1)$, find the eigenpair (λ_k, φ_k) such that

$$\begin{cases} -\big(\mu(y)\varphi_k'(y)\big)' + \sigma(y)\varphi_k(y) = \lambda_k w(y)\varphi_k(y) & \text{in } (0,1) \\ \chi_0\varphi_k(0) + \mu(0)\varphi_k'(0) = 0, \quad \chi_1\varphi_k(1) + \mu(1)\varphi_k'(1) = 0 \end{cases} \tag{14}$$

with $\chi_0, \chi_1 \in \mathbb{R}$, and where we assume the following regularity on the data:

$$\mu, \mu', \sigma, w \in C^0([0,1]) \quad \text{with} \quad \mu, w > 0 \text{ and } \sigma \geq 0 \text{ a.e. in } [0,1]. \tag{15}$$

The differential operator associated with equation (14) is linear, elliptic and self-adjoint. For $\chi_0 = \chi_1 = 0$, we obtain a fully Neumann problem (in particular, for $\sigma = 0$, problem (14) has multiple solutions - up to a constant - and this reflects in the fact that one of the eigenvalues is identically equal to zero with the associated eigenfunctions given by constants).

Analogously, the definition of a two-dimensional ($d = 3$) HiMod educated basis leads us to the SLE problem

$$\begin{cases} -\text{div}\big(\mu(\boldsymbol{y})\nabla\varphi_k(\boldsymbol{y})\big) + \sigma(\boldsymbol{y})\varphi_k(\boldsymbol{y}) = \lambda_k w(\boldsymbol{y})\varphi_k(\boldsymbol{y}) & \text{in } \gamma \\ \chi\varphi_k(\boldsymbol{y}) + \mu(\boldsymbol{y})\nabla\varphi_k(\boldsymbol{y}) \cdot \mathbf{n} = 0 & \text{on } \partial\gamma \end{cases} \tag{16}$$

with $\chi \in \mathbb{R}$ and $\mathbf{n}$ the unit outward normal vector to the boundary $\partial\gamma$, and where we assume the same regularity as in (15) on μ, σ and w.

In the following, we consider the coefficients μ and σ to be constant. The numerical methodology we present is however more general.

Notice that, in SLE problems (14) and (16), a constant reaction coefficient $\sigma \neq 0$ simply shifts the spectrum associated with the case $\sigma = 0$, while preserving the same eigenfunctions.

9

3.2 Approximability properties

We recall here some properties of SLE eigenfunctions. In the case of 1D SLE problem, most of these results can be found in Chapt. 5 of [9]. We illustrate the results in the general setting of interest for our problems.

Let $\mathcal{R}_m f$ denote the *residual* associated with the m-th truncated series in (11), namely

$$\mathcal{R}_m f(\boldsymbol{y}) = f(\boldsymbol{y}) - \mathcal{S}_m f(\boldsymbol{y}) = \sum_{k=m+1}^{+\infty} \hat{f}_k \varphi_k(\boldsymbol{y}).$$

Here, we investigate the convergence rate of the residual with respect to m and on the generic domain γ. To this aim, we first establish the dependence of the Fourier coefficient $\hat{f}_k$ on λ_k. In particular, when function f belongs at least to $H^2(\gamma)$, we can compute also the generalized Fourier series of Δf, whose k-th coefficient will be denoted by $\widehat{\Delta f}_k$. Coefficients $\widehat{\Delta f}_k$ will be employed to relate $\hat{f}_k$ with λ_k as stated in the following result.

Lemma 1 *Let φ_k be the eigenfunction, solution to problem* (16), *and let $f \in H^2(\gamma)$ be a generic function fulfilling the same boundary conditions as φ_k. Then, it holds*

$$\hat{f}_k = (f, \varphi_k)_{L^2_w(\gamma)} = -\frac{1}{\lambda_k}\widehat{\Delta f}_k \quad \forall k \geq 1. \tag{17}$$

Moreover, if $f \in H^{2p}(\gamma)$, with $p \geq 2$, and compatible boundary conditions are assigned in (16), *i.e., $f^{(2s)}$ satisfies the same boundary conditions as f, for any $s \leq p - 1$, then*

$$\hat{f}_k = \left(-\frac{1}{\lambda_k}\right)^p \widehat{\Delta^{(p)} f}_k \quad \forall k \geq 1, \tag{18}$$

where $\widehat{\Delta^{(p)} f}_k$ denotes the k-th coefficient of the generalized Fourier series of the p-Laplacian $\Delta^{(p)} f$.

Proof 3.1 *For the sake of simplicity, we prove the results above by assuming $w = 1$, $\mu = 1$ and $\sigma = 0$. By exploiting the differential problem in* (16) *and by integrating by parts twice, we get*

$$\begin{aligned}
\hat{f}_k &= \int_\gamma f(\boldsymbol{y})\varphi_k(\boldsymbol{y}) \, d\boldsymbol{y} = -\frac{1}{\lambda_k}\int_\gamma f(\boldsymbol{y})\Delta\varphi_k(\boldsymbol{y}) \, d\boldsymbol{y} \\
&= -\frac{1}{\lambda_k}\left[-\int_\gamma \nabla f(\boldsymbol{y}) \cdot \nabla\varphi_k(\boldsymbol{y}) \, d\boldsymbol{y} + \int_{\partial\gamma} \nabla\varphi_k(s) \cdot \boldsymbol{n} \, f(s) \, ds\right] \\
&= -\frac{1}{\lambda_k}\left[\int_\gamma \Delta f(\boldsymbol{y}) \, \varphi_k(\boldsymbol{y}) \, d\boldsymbol{y} + \int_{\partial\gamma} \nabla\varphi_k(s) \cdot \boldsymbol{n} \, f(s) \, ds - \int_{\partial\gamma} \varphi_k(s)\nabla f(s) \cdot \boldsymbol{n} \, ds\right] \\
&= -\frac{1}{\lambda_k}\int_\gamma \Delta f(\boldsymbol{y})\varphi_k(\boldsymbol{y}) \, d\boldsymbol{y} = -\frac{1}{\lambda_k}\widehat{\Delta f}_k.
\end{aligned} \tag{19}$$

In particular, since both φ_k and f satisfy the same boundary condition on $\partial\gamma$, the boundary terms in (19) are identically equal to zero. Indeed, we have

$$
\begin{aligned}
&\int_{\partial\gamma} \nabla\varphi_k(s) \cdot \boldsymbol{n}\, f(s)\, ds - \int_{\partial\gamma} \varphi_k(s)\nabla f(s) \cdot \boldsymbol{n}\, ds \\
=\ & \int_{\partial\gamma} -\chi\varphi_k(s)f(s)\, ds + \int_{\partial\gamma} \chi f(s)\varphi_k(s)\, ds = 0.
\end{aligned}
\tag{20}
$$

From (19) then (17) is proved. Moreover, since $\|\varphi_k\|_{L^2(\gamma)} = 1$, via the Cauchy-Schwarz inequality, we get the additional bound

$$
|\hat{f}_k| \le \frac{1}{\lambda_k}|f|_{H^2(\gamma)}.
$$

In addition, if we consider a function $f \in H^{2p}(\gamma)$ for some $p \ge 2$ and such that the r-Laplacian $\Delta^{(r)}f$ fulfills the same boundary conditions as f, for $0 \le r \le p-1$, we can iterate the same argument, to obtain

$$
-\widehat{\Delta^{(r)}f}_k = \frac{1}{\lambda_k}\widehat{\Delta^{(r+1)}f}_k.
\tag{21}
$$

By properly combining (19) with (21) for f regular enough, we obtain (18).

Let us analyze now the convergence of the residual $\mathcal{R}_m f$. We can state the following

Theorem 2 *Let φ_k be the eigenfunction, solution to problem (16), and let $f \in H^2(\gamma)$ satisfy the same boundary conditions as φ_k. Then, there exists a constant $C_{1,s}$ independent of m, such that*

$$
\|\mathcal{R}_m f\|_{H^s(\gamma)} \le C_{1,s}\left(\frac{1}{m+1}\right)^{\frac{2-s}{d-1}}|f|_{H^2(\gamma)},
\tag{22}
$$

for $s = 0,1$, and with $H^0(\gamma) \equiv L^2(\gamma)$. Moreover, if $f \in H^{2p}(\gamma)$, with $p \ge 2$ and compatible boundary conditions are assigned in (16), then there exists a constant $C_{2,s}$, independent of m, such that, for $s = 0,1$,

$$
\|\mathcal{R}_m f\|_{H^s(\gamma)} \le C_{2,s}\left(\frac{1}{m+1}\right)^{\frac{2p-s}{d-1}}|f|_{H^{2p}(\gamma)}.
\tag{23}
$$

Proof 3.2 *We first consider the case $s = 0$. By resorting to the Parseval's identity, we have*

$$
\|\mathcal{R}_m f\|_{L^2(\gamma)}^2 = \sum_{k=m+1}^{+\infty} \hat{f}_k^2.
$$

The properties of the SLE problem listed above guarantee that the right hand side converges to 0 for $k \to \infty$. In addition, the slowest term to converge is $\hat{f}_{m+1}$

11

since coefficients $\hat{f}_k$ inversely depend on λ_k. Thanks to Lemma 1 and by exploiting the Weyl formula, we have that, if $f \in H^2(\gamma)$ and satisfies the same boundary conditions of φ_k, then

$$||\mathcal{R}_m f||^2_{L^2(\gamma)} \le \left(\frac{1}{\lambda_{m+1}}\right)^2 \sum_{k=m+1}^{+\infty} \left[\widehat{\Delta f_k}\right]^2 \le \frac{C}{(m+1)^{\frac{4}{d-1}}} |f|^2_{H^2(\gamma)}, \quad (24)$$

with C depending on the domain, and where we have upper bounded the truncated series of the Laplacian of f via the $H^2(\gamma)$-seminorm of f. Analogously, if $f \in H^{2p}(\gamma)$ for some $p \ge 2$, and compatible boundary conditions are enforced in (16), we derive that

$$||\mathcal{R}_m f||^2_{L^2(\gamma)} \le \left(\frac{1}{\lambda_{m+1}}\right)^{2p} \sum_{k=m+1}^{+\infty} \left[\widehat{\Delta^{(p)} f_k}\right]^2 \le \frac{C}{(m+1)^{\frac{4p}{d-1}}} |f|^2_{H^{2p}(\gamma)}. \quad (25)$$

Now we select $s = 1$. We notice that the symmetric continuous and coercive bilinear form

$$a(\varphi_k, v) = \int_\gamma \mu \nabla \varphi_k(\mathbf{y}) \cdot \nabla v(\mathbf{y}) \, d\mathbf{y} + \int_{\partial\gamma} \chi \varphi_k(s) v(s) \, ds$$

associated with problem (16) for $\sigma = 0$ and defined in $H^1(\gamma)$, induces the scalar product $((w, v)) = a(w, v)$ and the norm $\|w\|^2_a = a(w, w)$ for any w and $v \in H^1(\gamma)$. In particular, the functions $\left\{\widetilde{\varphi}_k = \frac{\varphi_k}{\sqrt{\lambda_k}}\right\}_{k\in\mathbb{N}}$ form an orthonormal basis with respect to this scalar product[24]. The generalized *Fourier coefficients $\widetilde{f}_k = \left((f, \widetilde{\varphi}_k)\right)$ of f with respect to this basis can be easily related to the coefficients in (17) simply by exploiting problem (16) and integration by parts, as*

$$\widetilde{f}_k = \left((f, \widetilde{\varphi}_k)\right) = a(f, \widetilde{\varphi}_k) = \lambda_k(f, \widetilde{\varphi}_k) = \sqrt{\lambda_k}(f, \varphi_k) = \sqrt{\lambda_k}\,\hat{f}_k.$$

Via Parseval's identity and thanks to the coercivity of the bilinear form $a(\cdot, \cdot)$, we obtain

$$\alpha\|\mathcal{R}_m f\|^2_{H^1(\gamma)} \le \|\mathcal{R}_m f\|^2_a = \sum_{k=m+1}^{+\infty} \widetilde{f}_k^2 = \sum_{k=m+1}^{+\infty} \lambda_k \hat{f}_k^2,$$

with α the coercivity constant. The same arguments adopted in (24) and (25) lead to estimates

$$||\mathcal{R}_m f||^2_{H^1(\gamma)} \le \frac{\alpha^{-1}}{\lambda_{m+1}} \sum_{k=m+1}^{+\infty} \left[\widehat{\Delta f_k}\right]^2 \le \frac{C}{(m+1)^{\frac{2}{d-1}}} |f|^2_{H^2(\gamma)},$$

and

$$||\mathcal{R}_m f||^2_{H^1(\gamma)} \le \alpha^{-1}\left(\frac{1}{\lambda_{m+1}}\right)^{2p-1} \sum_{k=m+1}^{+\infty} \left[\widehat{\Delta^{(p)} f_k}\right]^2 \le \frac{C}{(m+1)^{\frac{4p-2}{d-1}}} |f|^2_{H^{2p}(\gamma)},$$

respectively, with C now depending also on the coercivity constant. This concludes the proof.

Remark 3.1 *For $p \to \infty$, estimate (23) yields spectral convergence. In the particular case of Neumann conditions, this means that a function f infinitely regular and with all the odd derivatives vanishing at the boundary is spectrally approximated by Fourier truncated series. This is a well known result recalled, for instance, in [9], Sect. 2.2, pag. 68.*

For the case with Neumann conditions in (16), we can prove an additional result under some regularity assumptions that however do not involve the boundary conditions of the derivatives of f. At the best of authors' knowledge, this result is non standard and it is reflected by our numerical findings.

Lemma 3 *Let φ_k be the eigenfunction, solution to problem (16) completed with Neumann boundary conditions (i.e., $\chi = 0$). If $f \in H^4(\gamma)$ and satisfies homogeneous Neumann boundary conditions as φ_k, then we have*

$$|\hat{f}_k| \leq C \frac{1}{\lambda_k^{3/2}} \|f\|_{H^4(\gamma)} \quad \forall k \geq 1, \tag{26}$$

with $C = C(\tau)$, τ being the constant associated with the trace inequality. In particular, if φ_k is bounded uniformly with k (as it happens for sinusoidal functions, Legendre polynomials as well as Bessel functions[2].), then the previous statement refines in

$$|\hat{f}_k| \leq C \frac{1}{\lambda_k^2} \|f\|_{H^4(\gamma)} \quad \forall k \geq 1. \tag{27}$$

We give the proof of the Lemma together with the proof of the following Corollary, for the sake of brevity. As Corollary we have the following results.

Corollary 4 *Under the assumptions of Theorem 2, there exists a constant $C_{3,s}$, independent of m, such that, for $s = 0, 1$,*

$$\|\mathcal{R}_m f\|_{H^s(\gamma)} \leq C_{3,s} \left(\frac{1}{m+1}\right)^{\frac{3-s}{d-1}} \|f\|_{H^4(\gamma)}. \tag{28}$$

If the basis functions are uniformly bounded, then there exists a constant $C_{4,s}$ independent of m such that

$$\|\mathcal{R}_m f\|_{H^s(\gamma)} \leq C_{4,s} \left(\frac{1}{m+1}\right)^{\frac{4-s}{d-1}} \|f\|_{H^4(\gamma)}. \tag{29}$$

Proof 3.3 *If $f \in H^4(\gamma)$, it is possible to mimic the procedure adopted in Lemma 1, by working directly on the coefficients of the generalized Fourier series for Δf,*

---

[2]Bessel functions are eigenfunctions for the Laplace eigenvalue problem[8] in 2D. Uniform boundedness is stated in [26]

to obtain

$$-\widehat{\Delta f}_k = -\int_\gamma \Delta f(\boldsymbol{y})\varphi_k(\boldsymbol{y})\,d\boldsymbol{y} = \frac{1}{\lambda_k}\int_\gamma \Delta f(\boldsymbol{y})\Delta\varphi_k(\boldsymbol{y})\,d\boldsymbol{y}$$

$$= \frac{1}{\lambda_k}\Big[\int_\gamma \Delta^{(2)}f(\boldsymbol{y})\varphi_k(\boldsymbol{y})\,d\boldsymbol{y} + \int_{\partial\gamma}\nabla\varphi_k(s)\cdot\boldsymbol{n}\,\Delta f(s)\,ds - \int_{\partial\gamma}\varphi_k(s)\nabla\big(\Delta f\big)(s)\cdot\boldsymbol{n}\,ds\Big] \tag{30}$$

where $\Delta^{(2)}$ denotes the bilaplacian operator. From (30) and since we assume Neumann boundary data, i.e., $\nabla\varphi_k\cdot\boldsymbol{n} = 0$, we have

$$-\frac{1}{\lambda_k}\widehat{\Delta f}_k = \frac{1}{\lambda_k^2}\Big[\int_\gamma \Delta^{(2)}f(\boldsymbol{y})\varphi_k(\boldsymbol{y})\,d\boldsymbol{y} - \int_{\partial\gamma}\varphi_k(s)\nabla\big(\Delta f\big)(s)\cdot\boldsymbol{n}\,ds\Big]. \tag{31}$$

By combining (19) with (31) together with the trace inequality yields the relation

$$|\hat{f}_k| \leq \frac{1+\tau^2\|\varphi_k\|_{H^1(\gamma)}}{\lambda_k^2}\|f\|_{H^4(\gamma)}$$

with τ the trace constant and keeping in mind that $\|\varphi_k\|_{L^2(\gamma)} = 1$. In addition, we have observed that $\|\varphi_k\|_{H^1(\gamma)} \simeq \sqrt{\lambda_k}$ that leads to (26). From (31), if $\|\varphi_k\|_{L^2(\partial\gamma)}$ is uniformly bounded with k, then (27) follows.

The corollary is an immediate consequence of (26) and (27) when we apply the arguments used in Theorem 2.

4 HiMod Educated Bases

The main contribution of this paper refers to using the SLE theory and SL eigenfunctions as informed or educated basis functions to incorporate general lateral boundary conditions prescribed on Γ_w in an essential fashion.

The educated HiMod (e-HiMod) procedure articulates in the following steps:

1. split the problem along the axial (1D) and the transverse ($(d-1)$D) directions, respectively;

2. solve the $(d-1)$-dimensional SLE problem associated with the symmetric part of the ADR operator on the transverse fiber γ, to obtain the modal basis $\{\varphi_k\}$;

3. assemble the block tridiagonal matrix associated with the 1D coupled problems (7), each block including the effect of the transverse dynamics;

4. solve system (7) and exploit the modal representation (5) to construct u_m^h.

Hereafter, we focus on step (2), by detailing the proposed approach in both 2D and 3D, separately. To simplify the discussion, westill assume μ, $\boldsymbol{\beta}$ and σ in (1) to be constant. Moreover, we complete problem (1) by prescribing for simplicity homogeneous Dirichlet boundary data on Γ_1 and Γ_2, and the homogeneous Robin condition $\mu\nabla u\cdot\mathbf{n} + \chi u = 0$ on Γ_w.

4.1 The 2D case in rectangular domains

Let us start by re-writing the weak form (1) by including the Robin condition: find $u = u(x, y) \in V \equiv H^1_{\Gamma_{1,2}}(\Omega)$ such that

$$
\int_0^L \int_0^1 \mu\left(\frac{\partial u}{\partial x}(x,y)\frac{\partial v}{\partial x}(x,y) + \frac{\partial u}{\partial y}(x,y)\frac{\partial v}{\partial y}(x,y)\right) dx\, dy + \int_0^L \chi u(x,1)v(x,1)dx
$$

$$
- \int_0^L \chi u(x,0)v(x,0)dx + \int_0^L \int_0^1 \left(\beta_1\frac{\partial u}{\partial x}(x,y)v(x,y) + \beta_2\frac{\partial u}{\partial y}(x,y)v(x,y)\right) dx\, dy
$$

$$
+ \int_0^L \int_0^1 \sigma u(x,y)v(x,y)dx\, dy = \int_0^L \int_0^1 f(x,y)v(x,y)dx\, dy \quad \forall v \in V,
$$

being $\Gamma_{1,2} = \Gamma_1 \cup \Gamma_2$. Now, we solve the SLE problem (14) with $w = 1$ and $\chi_0 = \chi_1 = \chi$ to generate the educated modal basis $\{\varphi_k\}$ with $k \in \mathbb{N}^+$ characterizing the HiMod approximation (5). The $L^2(\gamma)$-orthonormality of the eigenfunctions φ_k simplifies the first two HiMod coefficients in (8) to

$$
r^{11}_{k,j}(x) = \mu\delta_{jk}, \quad r^{10}_{k,j}(x) = \beta_1\delta_{jk}.
$$

The third HiMod coefficient reduces to

$$
r^{00}_{k,j}(x) = \int_0^1 \beta_2\varphi'_j(y)\varphi_k(y)dy + \lambda_j\delta_{jk}
$$

since, by exploiting problem (14), it holds

$$
\int_0^1 \left(\mu\varphi'_j(y)\varphi'_k(y) + \sigma\varphi_j(y)\varphi_k(y)\right)dy - \mu\left[\varphi'_j(y)\varphi_k\right]_0^1
$$

$$
= \int_0^1 \left(\mu\varphi'_j(y)\varphi'_k(y) + \sigma\varphi_j(y)\varphi_k(y)\right)dy + \chi[\varphi_j\varphi_k]_0^1 = \int_0^1 \lambda_j\varphi_j(y)\varphi_k(y)dy = \lambda_j\delta_{jk}.
$$

Therefore, the assembly cost of the HiMod matrix significantly reduces when resorting to an educated basis, at least for the case of constant coefficients. In addition, in the absence of a vertical convection (i.e., for $\beta_2 = 0$), the sparsity pattern is block-diagonal. This may introduce a significant cost reduction for the linear algebra.

Remark 4.1 *Non-homogeneous boundary conditions can be treated with appropriate lifting functions. These can be taken as a modal expansion of the boundary data. In addition, the case where different types of boundary conditions are prescribed on different portions of Γ_w can be considered as well by a domain decomposition approach.*

Remark 4.2 *In many cases, the solution to the 1D SLE problem* (14) *can be obtained analytically or after the numerical rootfinding of a nonlinear function[9]. For instance the eigenfunctions associated with problem*

$$-\varphi_k''(y) = \lambda_k \varphi_k(y) \qquad in\ (0,1)$$

completed with full homogeneous Dirichlet boundary conditions coincide with the sinusoidal functions, consistently with the modal basis adopted so far in a HiMod approximation[1]. For instance, for the mixed boundary conditions $\varphi_k(0) = 0$ and $\varphi_k'(1) + \chi \varphi_k(1) = 0$, the eigenvalues of the problem coincide with the roots of the nonlinear equation $\chi \tan(\lambda_k) + \lambda_k = 0$, while the eigenfunctions are given by $\varphi_k(y) = \sin(\lambda_k y)$. In both these cases, the basis functions are clearly uniformly bounded with k. When analytical solutions are not available, we compute the eigenpairs by numerical approximation.

4.2   The 3D case in slab domains

We hierarchically reduce now the ADR problem (1) in the parallelepiped domain of Fig. 1. For this purpose, we generalize the procedure in the previous section to a 3D setting. In particular, to identify the educated modal basis associated with the selected boundary conditions, we solve the SLE problem (16) on the transverse fiber γ by taking advantage of the Cartesian structure of Ω. In this way problem (16) can be turned into a pair of 1D SLE problems, whose solution can be computed analytically. For simplicity, we set $\sigma = 0$ since the reactive term just shifts the spectrum of the operator. Then, we factorize the eigenfunction in (16) as

$$\varphi_k(y,z) = \varphi_{y,p(k)}(y)\varphi_{z,q(k)}(z), \tag{32}$$

where $p(k)$ and $q(k)$ are indices related to the y- and to the z-coordinate, respectively used to identify the k-th 2D modal function. Factorization (32) leads to the 1D eigenvalue problems

$$\begin{cases} -\mu\varphi_{y,p}''(y) = \lambda_{y,p}\varphi_{y,p}(y) & in\ (0,L_y) \\ \mu\varphi_{y,p}'(0) + \chi\varphi_{y,p}(0) = 0, \\ \mu\varphi_{y,p}'(L_y) + \chi\varphi_{y,p}(L_y) = 0, \end{cases} \qquad \begin{cases} -\mu\varphi_{z,q}''(z) = \lambda_{z,q}\varphi_{z,q}(z) & in\ (0,L_z) \\ \mu\varphi_{z,q}'(0) + \chi\varphi_{z,q}(0) = 0, \\ \mu\varphi_{z,q}'(L_z) + \chi\varphi_{z,q}(L_z) = 0, \end{cases} \tag{33}$$

with $\lambda_{y,p}$ and $\lambda_{z,q}$ the eigenvalue associated with the eigenfunction $\varphi_{y,p}$ and $\varphi_{z,q}$, respectively. Thus, the eigenpair $\{\varphi_k(y,z), \lambda_k\}$ solution to the 2D problem (16) on the slice γ reads

$$\{\varphi_k(y,z), \lambda_k\} = \{\varphi_{y,p(k)}(y)\varphi_{z,q(k)}(z), \lambda_{y,p(k)} + \lambda_{z,q(k)}\}. \tag{34}$$

Consistently with the analysis of the previous section, the eigenvalues λ_k have to be sorted into a nondecreasing sequence. The identification of $p(k)$ and $q(k)$ to identify the correct eigenvalue in (34) of the sequence can be performed with the following algorithm hereafter denoted by ESA (Eigenvalue Sorting Algorithm). Let m be given. Then we perform the following steps.

i) For $k = 1$ we set $\lambda_1 = \lambda_{y,1} + \lambda_{z,1}$ with respect to y and z, respectively (i.e., $p(1) = 1$ and $q(1) = 1$ identify $k = 1$).

ii) While $k \leq m$ do

- compute $\lambda_{y,p(k)+1} + \lambda_{z,q(k)}$ and $\lambda_{y,p(k)} + \lambda_{z,q(k)+1}$ and store them in the list of the eigenvalues to examine;

- compute the minimal element in the list of the eigenvalues to examine: this will be assigned to λ_{k+1}; correspondingly we assign $p(k+1)$ and $q(k+1)$.

- Increment k.

A schematization of ESA is depicted in Fig. 5. In particular, the diagram refers to (33), for $L_y = \pi$ and $L_z = 3\pi/2$, completed with homogeneous Dirichlet boundary conditions, i.e., to a test case when the eigenvalues can be calculated exactly. The light grey boxes refer to eigenvalues already examined, while the white boxes identify the eigenvalues that have to be still checked. In the boxes we report three numbers with the following notation $(\lambda_{y,p(k)}, \lambda_{z,q(k)})\boldsymbol{\lambda_k}$; the numbers outside the boxes denote the index k.

As we recalled above, for the case $d = 3$ - when the fibers are 2D - eigenvalues are not necessarily simple. In the ESA, when this repetition occurs, either one of the repeated nodes or the other (in the dark grey boxes of Fig. 5) is removed from the list. For instance, after the detection of the simple eigenvalue $\lambda_4 = 5$, we obtain the next candidate 5.77 twice. One of the two occurrences (anyone of the two) needs to be eliminated from the tree.

Remark 4.3 *If the rectangular fiber γ is skewed with a dominant dimension between L_y and L_z, a different number of modal basis functions is expected along direction y and z, respectively. For instance, if $L_y \gg L_z$, the eigenvalues associated with z-direction are larger than the ones related to y-direction. Hence, less modal functions will be employed along z-direction than y-direction (recall that the truncation error of the approximating function scales with the inverse of the first eigenvalue of the integral, so a larger eigenvalue demands less modes). In particular, if the ratio between L_z and L_y is close to zero, out of m modes we will naturally select $m - 1$ in the y direction and 1 along z. In fact, along z one eigenfunction is enough and the tree of Fig. 5 becomes unbalanced, following only the y side of the branch.*

4.3 Error analysis

To perform the error analysis characterizing e-HiMod, we first compute the error associated with the modal discretization (semi-discrete problem), and then we include the error due to the finite element approximation of the axial dynamics.
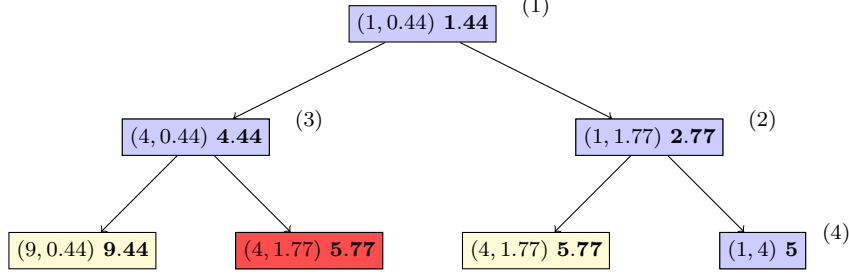
Figure 5: Schematization of ESA to select the 2D eigenvalues λ_k in (34).

We still refer to advection-diffusion-reaction problems.

As for the semi-discretization error, we have the following result. The letter C will denote a constant (not necessarily the same in each occurrence).

Theorem 5 *Let $u \in H^2(\Omega)$ be the solution to the full problem* (1)*, with $\Omega \subset \mathbb{R}^d$, and let $P_m u$ denote the projection of u onto the educated HiMod space V^m in* (3)*. Then, there exists a constant C, independent of m, such that*

$$||u - P_m u||_{H^s(\Omega)} \leq C \left(\frac{1}{m+1} \right)^{\frac{2-s}{d-1}} |u|_{H^2(\Omega)}, \tag{35}$$

for $s = 0, 1$ and with $H^0(\Omega) \equiv L^2(\Omega)$. Moreover, if $u \in H^{2p}(\Omega)$, with $p \geq 2$, and compatible boundary conditions (i.e. the $s-$Laplacian of u with $s \leq p - 1$ fulfills the same condition of u) complete the full problem, then there exists a constant C, independent of m, such that, for $s = 0, 1$,

$$||u - P_m u||_{H^s(\Omega)} \leq C \left(\frac{1}{m+1} \right)^{\frac{2p-s}{d-1}} ||u||_{H^{2p}(\Omega)}. \tag{36}$$

Proof 4.1 *By exploiting the density of the space V_∞ in $H^1(\Omega)$ for the modal representation of u, we have*

$$||u - P_m u||^2_{L^2(\Omega)} = \int_{\Omega_{1D}} \int_\gamma \left[\sum_{k=m+1}^{+\infty} u_k(x) \varphi_k(\mathbf{y}) \right]^2 d\mathbf{y} dx =$$

$$= \int_{\Omega_{1D}} ||(u - P_m u)(x)||^2_{L^2(\gamma)} dx.$$

Estimates (35) *and* (36) *now follow by Theorem 2 after identifying $\mathcal{R}_m f$ with $\big(u - P_m u \big)(x)$.*

Now, we consider the fully discretized solution u_m^h, obtained by completing the modal expansion with an approximation of the axial dynamics via finite elements of order r. We can prove the following

18

Theorem 6 *Let u be an $H^s(\Omega)$-function, with $s \geq 2$, solution to the full problem (1), with $\Omega \subset \mathbb{R}^d$. Then, the error associated with the e-HiMod approximation satisfies the* a priori *estimate (where C depends on the solution)*

$$\|u - u_m^h\|_{H^1(\Omega)} \leq C(h^q + m^{-l}) \tag{37}$$

with $q = \min(s - 1, r)$ and $l = 1/(d - 1)$. In particular, if $u \in H^{2p}(\Omega)$, with $p \geq 2$, and compatible boundary conditions complete the full problem, then $l = (2p - 1)/(d - 1)$.

Proof 4.2 *Via the Céa's Lemma and the triangle inequality, it follows*

$$\|u - u_m^h\|_{H^1(\Omega)} \leq \frac{M}{\alpha} \inf_{v_m^h \in V_m^h} \|u - v_m^h\|_{H^1(\Omega)} \leq \|u - v_m\|_{H^1(\Omega)} + \|v_m - v_m^h\|_{H^1(\Omega)} \tag{38}$$

where $v_m \in V_m$ is the semi-discrete counterpart of the generic e-HiMod function v_m^h, whereas M and α denote the continuity and the coercivity constants associated with the bilinear form in (1). Now, we identify v_m with $P_m u$. As a consequence, the second term on the right-hand side of (38) can be bounded by standard arguments. The thesis follows promptly from classical piecewise polynomial approximation results and Theorem 5.

In addition, we have the following result from Corollary 4.

Theorem 7 *Let $u \in H^4(\Omega)$ be the solution of (1) with Neumann lateral conditions (and Dirichlet conditions either on Γ_1 or Γ_2) and let $P_m u$ be defined as in Theorem 5. Then, the semi-discretization error for $s = 0, 1$ fulfills the bound*

$$\|u - P_m u\|_{H^s} \leq C \left(\frac{1}{m+1}\right)^{\frac{3-s}{d-1}} |u|_{H^4(\Omega)}, \tag{39}$$

where C is a constant independent of m. If the modal basis is uniformly bounded, then

$$\|u - P_m u\|_{H^s} \leq C \left(\frac{1}{m+1}\right)^{\frac{4-s}{d-1}} |u|_{H^4(\Omega)}. \tag{40}$$

The fully discrete e-HiMod solution then features the convergence rate

$$\|u - u_m^h\|_{H^1(\Omega)} \leq C(h^q + m^{-l})$$

with $q = \min(s - 1, r)$ and $l = (3 - s)/(d - 1)$ (or $l = (4 - s)/(d - 1)$ for uniformly bounded modal basis functions).

The proof follows the same arguments as in Theorems 5 and 6 and we omit it for the sake of brevity.

5 Numerical results

This section is devoted to the numerical assessment of the e-HiMod procedure. We consider both 2D and 3D test cases. The two-dimensional e-HiMod code is developed in Matlab, while the 3D tests are implemented in LifeV[22]. Numerical results will be tested against analytical solutions when available and finite element approximations on fine enough meshes otherwise.

In the e-HiMod approximation, we use linear finite elements (FE1) to discretize the supporting fiber combined with an educated modal basis to describe the transverse dynamics. Using higher order finite elements is currently under investigation.

5.1 2D qualitative assessment

We start investigating qualitatively the consistency of the e-HiMod procedure with a finite element solution on a fine mesh in absence of an analytical solution.

Let us consider the problem

$$
\begin{cases}
-\Delta u + \boldsymbol{\beta} \cdot \nabla u = f & \text{in } \Omega = (0,6) \times (0,1) \\
u = g_D & \text{on } \Gamma_{in} \\
\nabla u \cdot \boldsymbol{n} + \chi u = g_R & \text{on } \Gamma_{out} \\
\rho_1 \nabla u \cdot \boldsymbol{n} + \rho_2 u = 0 & \text{on } \Gamma_{w,up} \cup \Gamma_{w,down},
\end{cases}
\tag{41}
$$

where $\boldsymbol{\beta} = (20,0)^T$ represents a horizontal wind, the forcing term f models two elliptical sources localized in the left-portion of the domain, being $f(x,y) = \chi_{E_1 \cup E_2}(x,y)$, with $E_1 = \{(x,y) \in \Omega : (x-1.5)^2 + 0.4(y-0.25)^2 \leq 0.01\}$ and $E_2 = \{(x,y) \in \Omega : (x-1.5)^2 + 0.4(y-0.75)^2 \leq 0.01\}$. Conditions on Γ_w prescribe Robin, Dirichlet or Neumann data for different values of the parameters ρ_1, ρ_2. The latter can take different values on different portion of the boundary Γ_w, namely the upper and the lower sides, $\Gamma_{w,up} = [0,6] \times \{1\}, \Gamma_{w,down} = [0,6] \times \{0\}$. Here $\Gamma_{in} = \{0\} \times [0,1], \Gamma_{out} = \{6\} \times [0,1]$, (see Figure 6, left for a schematization of the test case). Finally, g_D and g_R are given functions and χ is a constant.

We test two combinations of boundary conditions on $\Gamma_{w,up}$ and $\Gamma_{w,down}$, i.e., Dirichlet/Robin and Robin/Robin data, respectively. At the intersection (corners) of the different portions of the boundary prescribed data are compatible. As reference solution we take FE1 approximation computed on a structured uniform grid with mesh size $h_x = h_y = 0.0025$. For the e-HiMod simulations we adopt a FE1 discretization along Ω_{1D} with uniform length $h_x = 0.01$, while varying the number of educated modes along γ.

Dirichlet/Robin

We assign the Robin condition $\nabla u \cdot \boldsymbol{n} = -3(u - 0.06)$ on $\Gamma_{w,down}$, and Dirichlet conditon $u = 0.05$ on $\Gamma_{w,up}$. In Figure 7, top we show the contour plot of the reference FE1 approximation. The Robin data on $\Gamma_{w,down}$ warps downward the
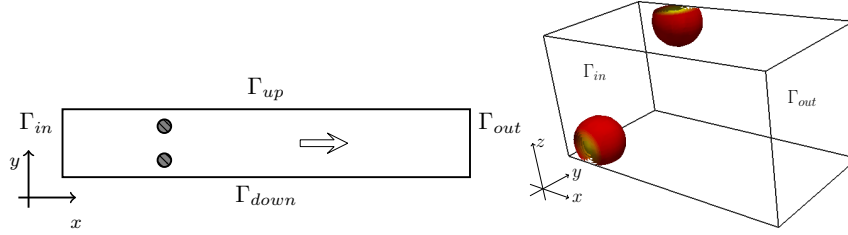
Figure 6: Schematization of the test case setting for the 2D (left) and the 3D (right) e-HiMod verification.

horizontal dynamics induced by the wind, so the effect of the two forcing terms on the solution is different and clearly detectable.

We compute the e-HiMod approximation by gradually increasing the modal index m. We adopt the notation e-Himod(m) to denote the hierarchically reduced solution associated with m educated modal functions. Figure 7 shows the contour plot of the e-HiMod(m) approximation, for $m = 2, 4, 8$. As expected, the quality of the reduced solution improves when m increases. For $m = 8$ the solution fully overlaps to the reference one.
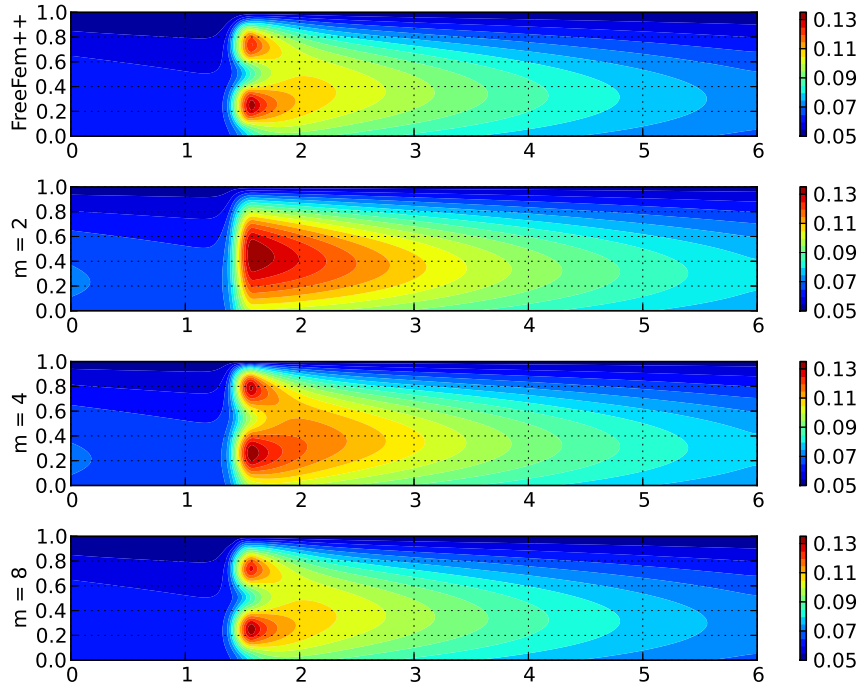
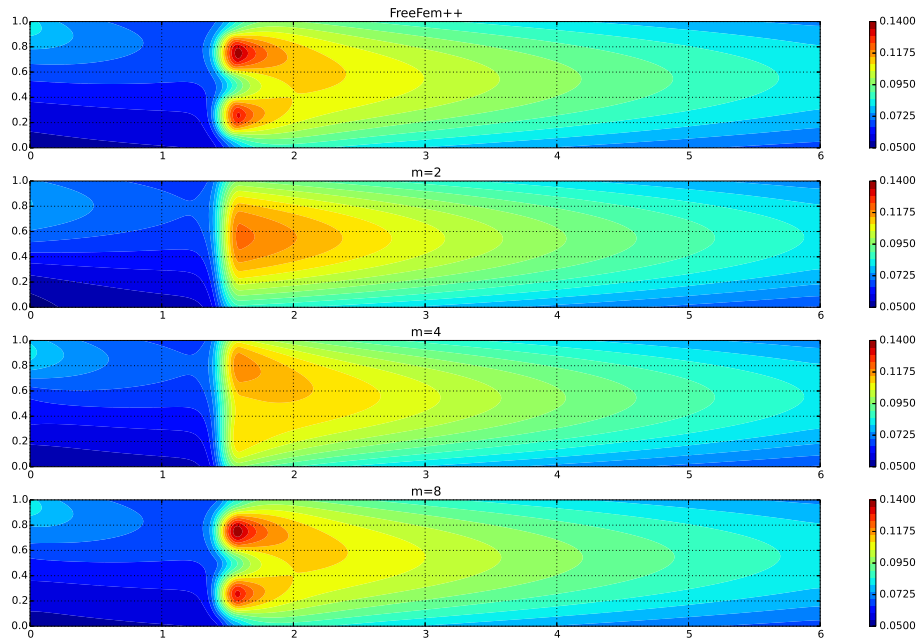
Figure 7: Dirichlet/Robin BC: reference FE1 solution (top); e-HiMod(m) reduced solution for $m = 2, 4, 8$ (second-fourth row).

Robin/Robin

We now assign non-homogeneous Robin conditions on both $\Gamma_{w,up}$ and $\Gamma_{w,down}$, namely we impose $\nabla u \cdot \boldsymbol{n} = -3(u - 0.06)$ on $\Gamma_{w,up}$ and $\nabla u \cdot \boldsymbol{n} = -3(u - 0.05)$ on $\Gamma_{w,down}$ respectively. In Figure 8 we compare the e-HiMod(m) approximation corresponding to $m = 2, 4, 8$ (second-fourth row) with the reference solution.

Due to the particular nature of the (nontrivial) solution, in this case $m = 4$ still provides an inaccurate solution, while the inclusion of four more modes to have $m = 8$ provides an accurate solution.

Figure 8: Robin/Robin BC: reference FE1 solution (top); e-HiMod(m) reduced solution for $m = 2, 4, 8$ (second-fourth row).

5.2 Educated vs non-educated modal bases

This section highlights the added value provided by an educated modal basis with respect to a standard Fourier basis. For the sake of simplicity, this check is per-
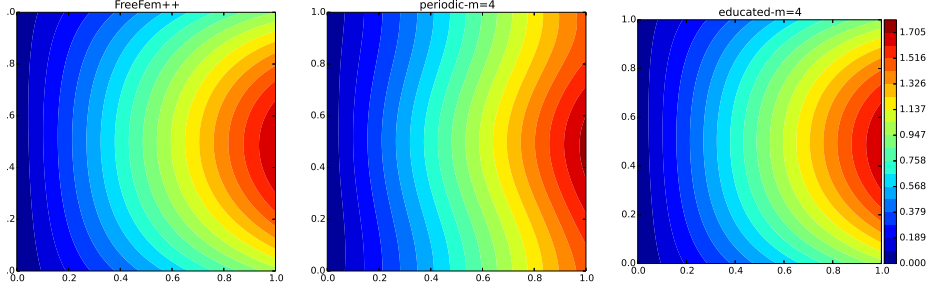
Figure 9: Exact solution to the ADR problem (42) (left); HiMod approximation based on $\mathcal{B}_4$ (center) and on an educated basis with four modes (right).

formed in a 2D setting. To this aim, we consider the ADR problem

$$
\begin{cases}
-\Delta u + \boldsymbol{\beta} \cdot \nabla u + \sigma u = f & \text{in } \Omega = (0,1)^2 \\
u = u_{ex} & \text{on } \Gamma_{in} = \{0\} \times [0,1] \\
\nabla u \cdot \mathbf{n} = \nabla u_{ex} \cdot \mathbf{n} & \text{on } \Gamma_{out} = \{1\} \times [0,1] \\
\nabla u \cdot \mathbf{n} + 3u = 0 & \text{on } \Gamma_w = \Gamma_{w,up} \cup \Gamma_{w,down} = [0,1] \times \{0,1\},
\end{cases}
\tag{42}
$$

with $\boldsymbol{\beta} = (20,0)^T$ and $\sigma = 2$. The source term is selected so that the analytical solution reads

$$
\begin{aligned}
u_{ex} &= xy + x + y + \exp(2xy - y) - 1 \\
&\quad - y^2 \big[2x + \exp(2x - 1) + 0.1((4x - 6)\exp(2x - 1) - 6x + 2) \big].
\end{aligned}
$$

In Figure 9, left we provide the contour plot of u_{ex}.

One possible approach leads us to employ a standard Fourier series $\mathcal{B}_m = \{1, \cos(j\pi y), \sin(j\pi y)\}_{j=1}^m$ and a natural treatment of the boundary conditions. This is expected to introduce some boundary layer in the error as opposed to the essential treatment of the same conditions with an educated basis. This is confirmed by the contour plots of Figure 9, center and right associated with the basis $\mathcal{B}_4$ and with the e-HiMod(4) solution, respectively. While this last approximation matches the exact solution, the standard HiMod solution based on $\mathcal{B}_4$ exhibits a significant discrepancy to u_{ex}.

We compare the convergence of the two HiMod approximations. In Figure 10 we show the global error rate in the $L^2(\Omega)$- (left) and the $H^1(\Omega)$-norm (right), for both the educated and the non-educated modal bases. Convergence is attained by both, even though the convergence rate of $\mathcal{B}_m$ is definitely slower vs. the e-HiMod approach. In particular, the Fourier basis leads to a linear convergence for the $L^2(\Omega)$-norm, and sub-linear convergence rate for the $H^1(\Omega)$-norm. No sensitivity with respect to h can be appreciated, suggesting that the modal error dominates. Theorem 6 predicts for the e-HiMod solution a quadratic and a linear convergence for the $L^2(\Omega)$- and the $H^1(\Omega)$-norm of the global error, respectively. Actually,
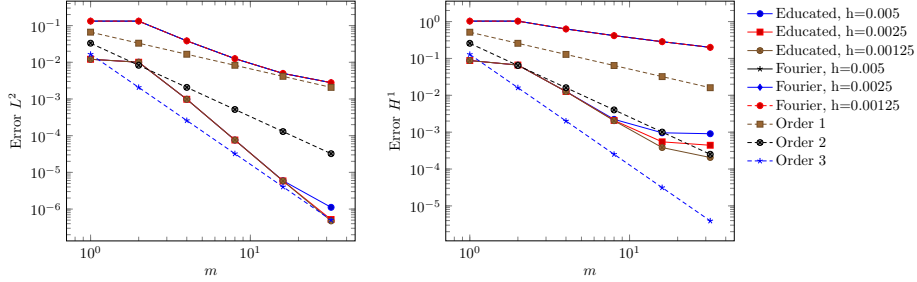
23

Figure 10: Educated vs non-educated bases. Comparison of the convergence rate of the global error for different discretization steps: $L^2(\Omega)$-norm (left) and $H^1(\Omega)$-norm (right).

results in Figure 10 slightly outperform the expected convergence rate in the range of modes selected, while the finite element error confirms the theory.

5.3 Comparison with a 1D model reduction

Let us compare the e-HiMod procedure with a standard 2D FE approximation and the reduced model considered in [21]. We compare the degrees of freedom of the different approaches. We consider the same equations of Section 5.1 with the source term $f = 10\chi_{F_1 \cup F_2}(x, y)$, with $F_1 = \{(x, y) \in \Omega : (x - 3)^2 + 0.4(y - 0.25)^2 \leq 0.01\}$ and $F_2 = \{(x, y) \in \Omega : (x - 1.5)^2 + 0.4(y - 0.75)^2 \leq 0.01\}$ (the two sources are now misaligned).

When the leading dynamics is aligned with the supporting 1D fiber, the e-HiMod approach reduces the number of dof without giving up accuracy. To show this, we compute a high-resolution FE1 approximation based on a uniform structured mesh of sizes $h_x = 0.01$, $h_y = 0.01$ (Figure 11, first row); a low-resolution FE1 approximation by increasing h_y to 0.2 (Figure 11, second row); the e-HiMod(m) approximation associated with $m = 1$ (Figure 11, fourth row) and $m = 5$ (Figure 11, fifth row) with $h_x = 0.01$ in both the cases. Consequently, the number of degrees of freedom of the four approximations is 60000, 3000, 600 and 3000, respectively. The e-HiMod(5) solution perfectly matches the high-resolution FE1 approximation albeit with a 20 times smaller system. Conversely, the low-resolution FE solution demands the same number of dof as e-HiMod(5) but with a lower accuracy. Finally, as expected, the e-HiMod(1) model is too coarse due to the limited transverse information carried by a single mode.

We stress that our primary goal is not to improve the efficiency of a 3D solver but to provide a solver to be used in network of pipes to capture systemic dynamics yet able to compute locally refined solutions. In this respect, we aim at comparing the e-HiMod approach with purely 1D solvers, where the dependence on the vertical coordinate is postulated *a priori* as well as with geometric multiscale models, where the local refinement is obtained by using dimensionally heterogeneous models[2]. To assess this point, in [21], we propose a 1D reduced model for an
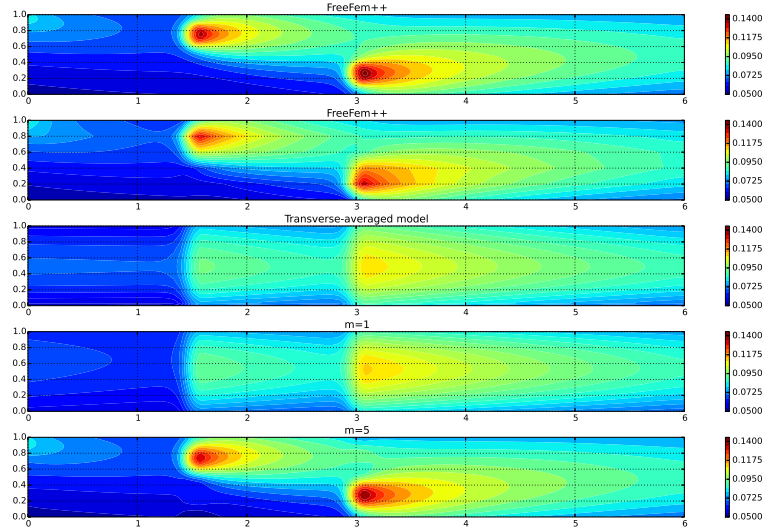
24

Figure 11: Robin/Robin BC. Comparison among 2D FE1 discretizations (first and second row), the transverse-averaged ADR model (third row), and the e-HiMod(1) and e-HiMod(5) approximations (fourth and fifth row).

ADR problem by averaging the corresponding 2D model along the transverse direction. In particular, we assume that the solution u to (41) may be expanded as $u(x, y) = \bar{u}(x)p(y)$, where $\bar{u}$ is the mean of u along the fiber γ, while p is such that $\int_0^1 p(y)dy = 1$. In general, p is assigned when setting the 1D reduced model. In [21] this transverse-averaged ADR model is used in a geometric multiscale formulation and compared with a HiMod approximation. We make here the point that e-HiMod provides a much more flexible approach yet retaining a good level of local accuracy by a judicious selection of m. We compute the transverse-averaged solution by preserving the partition along the x-axis of size $h_x = 0.01$ resulting in 600 dof. Profile p is retrieved from the high-resolution FE1 approximation. The quality of the corresponding reduced model is poor as shown in Figure 11, third row. The solution is even less accurate than the e-HiMod(1) approximation.

5.4 Convergence analysis

When assessing the convergence rate of the e-HiMod approximation, we will select a step h small enough to emphasize the modal error; alternatively, a large number of modes m to outline the 1D finite element approximation error. We consider both 2D and 3D cases. All the convergence graphs provided hereafter are log-log plots.

5.4.1 The 2D case

Dirichlet/Robin

The first case test solves on the unit square the advection-diffusion-reaction problem, completed with homogeneous Dirichlet boundary conditions on the upper side and with Robin boundary conditions on the lower side,

$$
\begin{cases}
-\Delta u + \boldsymbol{\beta} \cdot \nabla u + \sigma u = f & \text{on } \Omega = (0,1)^2 \\
u = u_{ex} & \text{on } \Gamma_{in} = \{0\} \times [0,1] \\
u = 0 & \text{on } \Gamma_{w,up} = [0,1] \times \{1\} \\
\nabla u \cdot \boldsymbol{n} + u = 3 & \text{on } \Gamma_{w,down} = [0,1] \times \{0\} \\
\nabla u \cdot \boldsymbol{n} = 0 & \text{on } \Gamma_{out} = \{1\} \times [0,1],
\end{cases}
\tag{43}
$$

with $\boldsymbol{\beta} = [20,0]^T$ and $\sigma = 2$. The source term is chosen such that the analytical solution is $u_{ex} = 4y^2(1-y)(0.75+8x^2y+8xy^2)(x-1)^2+(1-y)^2$ (see Figure 12, left).
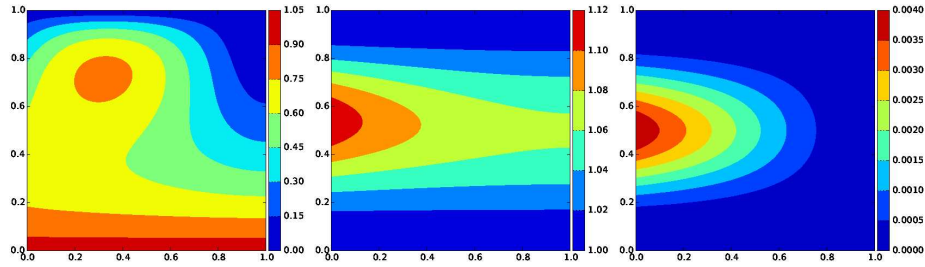

Figure 12: Exact solution to problem (43) completed with Dirichlet/Robin (left) and Neumann/Neumann (center) BC, and to the superconvergent test case (right).

The results of the convergence analysis are summarized in Figure 13 and quantified in Table 1 and 2, where we provide the global error $u-u_m^h$ for the $L^2(\Omega)$- and the $H^1(\Omega)$-norm, respectively. The step size h is gradually halved starting from the value 0.1; conversely, the modal index is doubled, starting from a single mode through $m = 32$. For h small enough, modal approximation slightly outperforms the expected convergence rates (error reduction factors are about 5 and to 2.5 vs. the expected 4 and 2). This is most likely related to the regularity of the solution. For the largest values of h, we have a stagnation of the error in the H^1-norm. The error dependence on h can be evidenced only for high values of m, as the modal error dominates.

Neumann/Neumann

We test the results of Theorem 7 for Neumann boundary data. For this purpose, we replace in (43) the conditions on $\Gamma_{w,up}$ and $\Gamma_{w,down}$ with a homogeneous Neumann
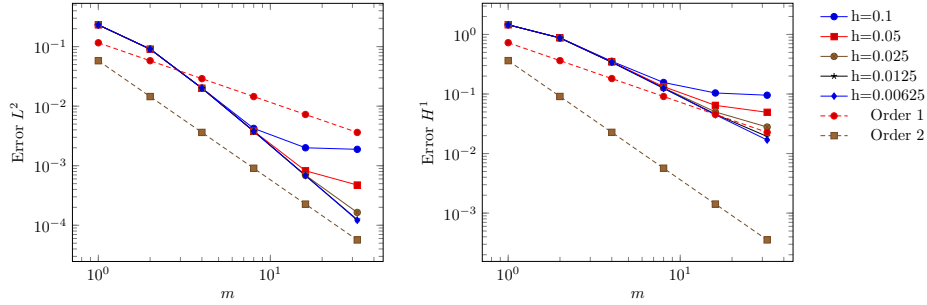
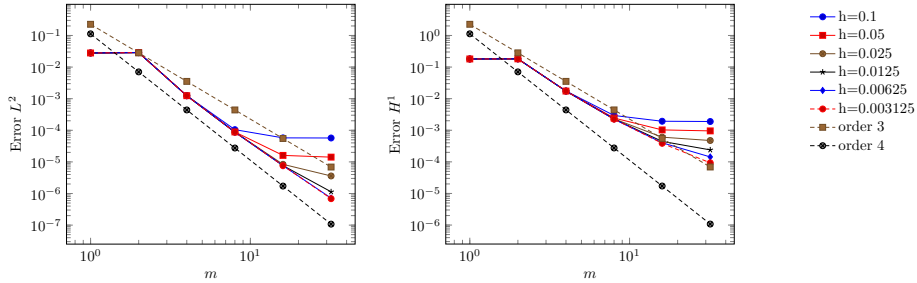Figure 13: 2D Dirichlet/Robin BC. Convergence of the global error for different discretization steps: $L^2(\Omega)$-norm (left) and $H^1(\Omega)$-norm (right).

m	h=0.1	h=0.05	h=0.025	h=0.0125	h=0.00625
1	2.32e-01	2.32e-01	2.32e-01	2.32e-01	2.32e-01
2	9.09e-02	9.08e-02	9.08e-02	9.08e-02	9.08e-02
4	2.01e-02	2.00e-02	2.00e-02	2.00e-02	2.00e-02
8	4.23e-03	3.82e-03	3.79e-03	3.79e-03	3.79e-03
16	2.00e-03	8.22e-04	6.91e-04	6.83e-04	6.82e-04
32	1.88e-03	4.74e-04	1.64e-04	1.24e-04	1.21e-04

Table 1: 2D Dirichlet/Robin BC: global error with respect to the $L^2(\Omega)$-norm.

data, while preserving the condition on Γ_{in} and the free-flux condition on Γ_{out}. The exact solution reads now $u_{ex} = y^2(1-y)^2 \exp\big(\sin(20y^3(1-y)^2(x-1)^2)\big)$ (see Figure 12, center). Theorem 7 predicts order 4 and 3 with respect to the $L^2(\Omega)$- and the $H^1(\Omega)$-norm, respectively. In Figure 14 we provide the plot of the global error as a function of m and for decreasing values of h. The plots associated with different mesh sizes are perfectly overlapped until 16 educated modes are used. The error stagnates except for the smallest values of h, showing a dominance of the finite element discretization error. For $h = 0.0125, 0.00625, 0.003125$, the $L^2(\Omega)$-norm of the error shows the expected order of convergence, while the choices $h = 0.00625$, $h = 0.003125$ show the rate predicted by Theorem 7 for the $H^1(\Omega)$-norm. Finally, as for the previous boundary data, the $H^1(\Omega)$-norm exhibits a minor sensitivity to the step size h.

Compatible conditions

In this test case we solve problem (43) by assigning homogeneous Dirichlet boundary conditions on $\Gamma_{w,up} \cup \Gamma_{w,down}$. Thus, the exact solution coincides with $u_{ex} = y^4(1-y)^4 e^x(x-1)^2$ (see Figure 12, right). The peculiar feature of this function is that it satisfies compatible boundary conditions. In particular, the Laplacian of u

m	h=0.1	h=0.05	h=0.025	h=0.0125	h=0.00625
1	1.45e+00	1.45e+00	1.45e+00	1.45e+00	1.45e+00
2	8.77e-01	8.74e-01	8.73e-01	8.73e-01	8.73e-01
4	3.55e-01	3.45e-01	3.43e-01	3.42e-01	3.42e-01
8	1.56e-01	1.33e-01	1.27e-01	1.25e-01	1.25e-01
16	1.04e-01	6.45e-02	5.01e-02	4.58e-02	4.49e-02
32	9.54e-02	4.93e-02	2.79e-02	1.93e-02	1.69e-02

Table 2: 2D Dirichlet/Robin BC: global error with respect to the $H^1(\Omega)$-norm.

Figure 14: 2D Neumann/Neumann BC. Convergence of the global error for different discretization steps: L^2-norm (left) and $H^1(\Omega)$-norm (right).

is identically equal to zero on $\Gamma_{w,up}$ and $\Gamma_{w,down}$. For such a function, we expect a superconvergent trend when evaluating the global error with respect to the $L^2(\Omega)$- and the $H^1(\Omega)$-norm, consistently with the results in Theorem 6. We confirm this behavior in Figure 15. The convergence rate for the $L^2(\Omega)$-norm is about four, as stated in (37), for h sufficiently small. For the $H^1(\Omega)$-norm finite element error induces stagnation, preventing to appreciate the expected modal error convergence rate.
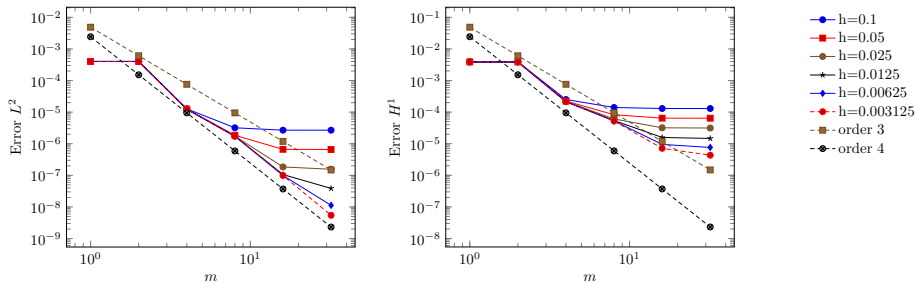

Figure 15: 2D compatible BC. Convergence of the global error for different discretization steps: $L^2(\Omega)$-norm (left) and $H^1(\Omega)$-norm (right).

28

5.4.2 The 3D case

We extend the numerical investigation on the convergence rate characterizing the e-HiMod approach to a 3D setting, in particular by focusing on the $L^2(\Omega)$-norm. As for the 2D case, we consider different choices for the boundary conditions to be assigned on Γ_w.

Dirichlet

We solve problem (9) on a slab with $\boldsymbol{\beta} = (5, 1, 1)^T$ and $\sigma = 3$. To begin with, we assign homogeneous Dirichlet data on the whole Γ_w, while we assign a Dirichlet data on Γ_1 and homogeneous Neumann boundary conditions on Γ_2. In particular, we select the source term and the Dirichlet condition on Γ_1 so that the exact solution is $u_{ex}(x, y, z) = 10^7 y(0.1 - y)z(0.1 - z)(x - 0.2)^2 \exp(2yz(0.2 - x)^2)$. As for the 2D analysis, we make different choices for the (uniform) spacing step along the supporting fiber Ω_{1D} and then, for each selected h, we gradually increase the number of modal functions.

Figure 16, left shows the trend of the global error for five choices of h. The modal order of convergence predicted for the $L^2(\Omega)$-norm by the theory in Section 4 is one. This is approximatively what we infer from the results when the finite element error does not dominate.
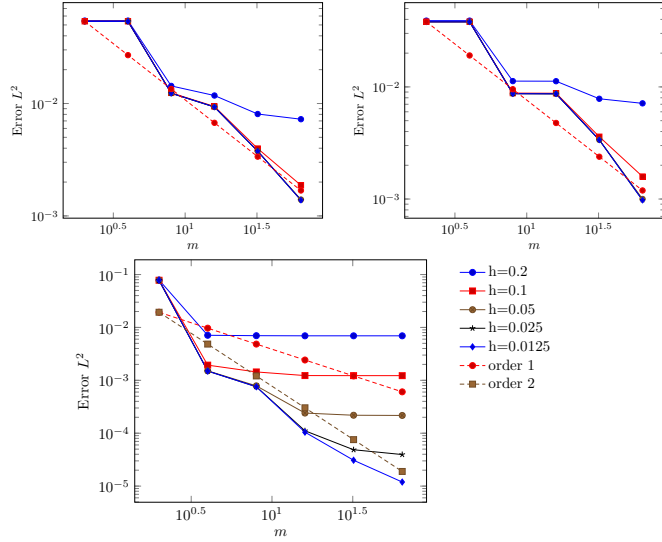

Figure 16: 3D convergence analysis of the global error with respect to the $L^2(\Omega)$-norm and for different discretization steps: Dirichlet (left), Dirichlet/Robin (center) and Robin (right) BC.

Dirichlet/Robin

We solve on the cube $\Omega = (0, 0.1)^3$ the standard Poisson problem by assigning a homogeneous Dirichlet data on $\Gamma_{w,up}$, the homogeneous Robin condition $\nabla u \cdot \mathbf{n} + 3.345u = 0$ on $\Gamma_{w,left}, \Gamma_{w,right}$ and $\Gamma_{w,down}$. The source term is selected such that the exact solution coincides with $u_{ex}(x, y, z) = 10^5(0.1 - x)^2 z(0.1 - z) \exp\left(70y^2/(xz + 1) - 140y^3/(0.3(xz + 1)) - 3.345(0.1 - 2y)^2/(0.4\mu)\right)$. As shown in Figure 16, center the $L^2(\Omega)$ norm of the error has a rate very similar to the fully Dirichlet case, showing how the educated approach does successfully extend the results found for the Dirichlet case. For m sufficiently large and for h small enough, we obtain the expected rate of convergence.

Robin

We modify the previous test case by assigning now a full Robin boundary condition $\nabla u \cdot \mathbf{n} + 4.456u = 0$ on the entire lateral surface. We observe more sensitivity to the selected step size h with respect to the previous choices of boundary conditions (compare the panel in Figure 16, right with the two others). To check the modal convergence, we analyze the plots associated with $h = 0.0125$ with essentially the expected linear rate.

5.5 The backward facing step test case

We conclude this section by analyzing the robustness of the proposed approach on a more complex geometry, both in 2D and in 3D.

5.5.1 The 2D case

We identify the computational domain Ω with the L-shaped portion of the Cartesian plane given by $\Omega_q \setminus \Omega_l$, with $\Omega_q = (0, 2) \times (-1, 1)$ and $\Omega_l = (0, 1) \times (-1, 0)$. Moroever, we distinguish the following portions of the boundary $\partial\Omega$: $\Gamma_{in} = \{0\} \times [0, 1]$ and $\Gamma_{out} = \{2\} \times [-1, 1]$ coinciding with the inlet and the outlet border, respectively; $\Gamma_{w,up} = [0, 2] \times \{1\}$ and $\Gamma_{w,down} = [1, 2] \times \{-1\} \cup \{1\} \times [-1, 0]$ to denote the upper and lower portion of the boundary, respectively. On this domain we solve the ADR problem

$$\begin{cases} -\Delta u + \boldsymbol{\beta} \cdot \nabla u = f & \text{in } \Omega \\ u = y(1 - y) & \text{on } \Gamma_{in} \\ \nabla u \cdot \mathbf{n} = 0 & \text{on } \Gamma_{out} \\ \nabla u \cdot \mathbf{n} + u = 0 & \text{on } \Gamma_{w,up} \\ u = 0 & \text{on } \Gamma_{w,down}, \end{cases} \tag{44}$$

where the source term is $f(x, y) = 10\chi_{G_1 \cup G_2}(x, y)$, with $G_1 = \{(x, y) \in \Omega : (x - 1.5)^2 + 0.4(y - 0.25)^2 \le 0.01\}$ and $G_2 = \{(x, y) \in \Omega : (x - 1.5)^2 + 0.4(y - $
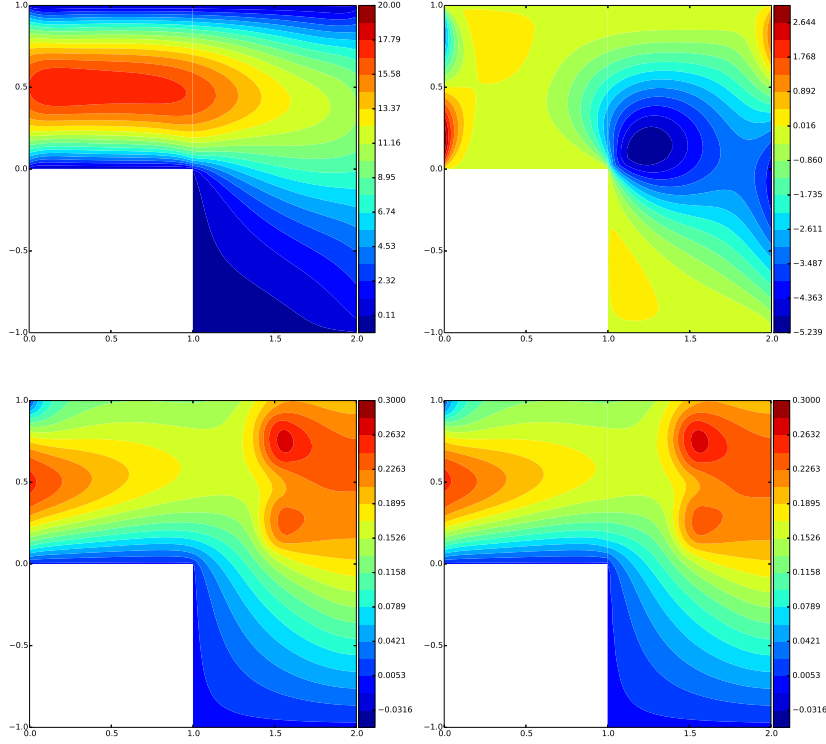
Figure 17: 2D backward facing step: advective field $\boldsymbol{\beta}$ x-component (top left) and y-component (top right); reference FE1 solution (bottom left); piecewise e-HiMod$(8, 20)$ reduced solution (bottom right).

$0.75)^2 \leq 0.01\}$, while the advective field $\boldsymbol{\beta}$ is the solution to the Stokes problem

$$
\begin{cases}
-\nabla \cdot \sigma(\boldsymbol{\beta}, p) = 0 & \text{in } \Omega \\
-\nabla \cdot \boldsymbol{\beta} = 0 & \text{in } \Omega \\
\sigma(\boldsymbol{\beta}, p)\mathbf{n} = 5\mathbf{n} & \text{on } \Gamma_{in} \\
\sigma(\boldsymbol{\beta}, p)\mathbf{n} = 0\mathbf{n} & \text{on } \Gamma_{out} \\
\boldsymbol{\beta} = \mathbf{0} & \text{on } \Gamma_w = \Gamma_{w,up} \cup \Gamma_{w,down},
\end{cases}
\tag{45}
$$

with $\sigma = \nu(\nabla\boldsymbol{\beta} + \nabla\boldsymbol{\beta}^T) - pI$ the stress rate tensor depending on the velocity $\boldsymbol{\beta}$ and on the pressure p, and with $\nu > 0$ the kinematic viscosity and I the identity matrix. The field $\boldsymbol{\beta}$ has been approximated on the same mesh employed to compute the solution of (44) and via a P2-P1 finite element scheme (see Figure 17, top).

Figure 17, bottom left shows the contour plots of the FE1 approximate solution computed on a structured 2D mesh of uniform step sizes $h_x = h_y = 0.01$. To approximate problem (44) via an e-HiMod procedure, we resort to the piecewise Hi-Mod formulation[7]. Following this approach, we split the computational domain

31

into two subregions to apply a standard HiMod reduction on each of them. More precisely we subdivide the L-shaped domain into the subdomains $\Omega_1 = (0,1)^2$ and $\Omega_2 = (1,2) \times (-1,1)$. Following [7, 12], we resort to a domain decomposition iterative method. In particular, we adopt a relaxed Dirichlet/Neumann scheme in correspondence with the interface $\Gamma = \{1\} \times (0,1)$ between Ω_1 and Ω_2. We employ 8 and 20 educated modal functions on Ω_1 and Ω_2, respectively while introducing a uniform subdivision along the supporting fiber Ω_{1D} of steplength $h_x = 0.01$.

The e-HiMod$(8, 20)$ reduced solution in Figure 17, bottom right compares very well with the full finite element solution (yet with a significant reduction of dof) even in capturing transverse dynamics induced by the geometry that would be dropped in a purely 1D model.

5.5.2 The 3D case

We solve on the 3D domain $\Omega = \Omega_Q \setminus \Omega_L$, with $\Omega_Q = (0,2) \times (0,1) \times (0,2)$ and $\Omega_L = (0,1)^2 \times (1,2)$, the advection-diffusion problem

$$
\begin{cases}
-\Delta u + \boldsymbol{\beta} \cdot \nabla u = f & \text{in } \Omega \\
u = g & \text{on } \Gamma_{in} \\
\nabla u \cdot \mathbf{n} = 0 & \text{on } \Gamma_{out} \\
u = 0 & \text{on } \Gamma_w,
\end{cases}
\tag{46}
$$

where, for the sake of simplicity, we select a constant field, $\boldsymbol{\beta} = (20, 0, 7)^T$, and with $\Gamma_1 = \{x = 0\} \times (0,1)^2$, $\Gamma_2 = \{x = 2\} \times (0,1) \times (0,2)$, $\Gamma_w = \partial\Omega \setminus (\Gamma_{in} \cup \Gamma_{out})$. The forcing term is localized in correspondence with three spherical regions, being $f(x, y, z) = 20\chi_{S_1 \cup S_2 \cup S_3}(x, y, z)$, with $S_1 = \{(x, y, z) \in \Omega : (x - 0.7)^2 + (y - 0.3)^2 + (z - 0.3)^2 \le 0.1\}$, $S_2 = \{(x, y, z) \in \Omega : (x - 1.3)^2 + (y - 0.5)^2 + (z - 0.5)^2 \le 0.1\}$, $S_3 = \{(x, y, z) \in \Omega : (x - 1.2)^2 + (y - 0.6)^2 + (z - 1.5)^2 \le 0.1\}$. Figure 18, left shows the contour plot of the reference 3D FE1 approximation computed on a structured mesh of uniform step sizes $h_x = h_y = h_z = 1/30$. In particular, the plot refers to the transverse section at $y = 0.5$.

For HiMod we resort to a piecewise hierarchical model reduction applied to the subdomains $\Omega_1 = (0,1)^3$ and $\Omega_2 = (1,2) \times (0,1) \times (0,2)$. We use sinusoidal basis functions in a tensor product setting of the 1D SLE problems on each subdomain. A uniform 1D discretization of step size $h_x = 1/30$ is employed on the supporting fiber Ω_{1D}. We consider the two cases of 100 and 200 modes in the two subdomains. The relaxed Dirichlet/Neumann scheme converges after a few iterations and provides the HiMod approximations in Figure 18, center (for $m = 100$) and right (for $m = 200$). The HiMod(100) solution is already comparable with the reference one in Figure 18, left despite a lack of accuracy along the edge $E = \{x = 1\} \times (0,1) \times \{z = 1\}$. The matching of the two reduced solutions along E is a challenging task. In fact, the modal functions on Ω_1 are identically equal to zero on $(0,1)^2 \times \{z = 1\}$ due to the Dirichlet data, whilst the modes involved in Ω_2 are free to assume any value across $(1,2) \times (0,1) \times \{z = 1\}$.
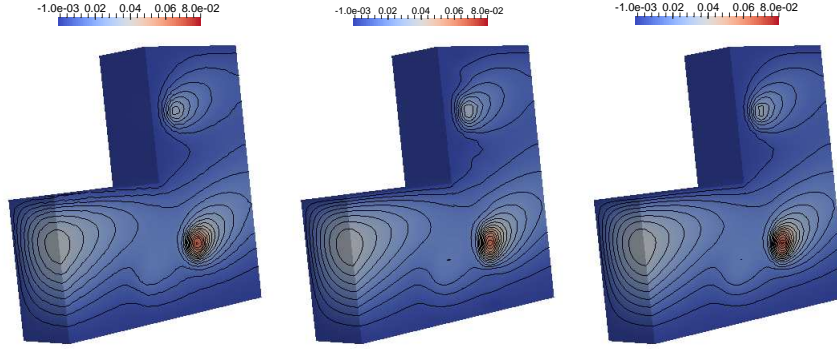
Figure 18: 3D backward facing step, full homogeneous Dirichlet BC: reference FE1 solution (left); HiMod(m) reduced solution for $m = 100$ (center) and $m = 200$ (right).

As expected, the mismatch between the two approximations diminishes when we move away from E since no boundary data constrains the projection of a HiMod basis onto the other one. This drawback completely disappears when dealing with the HiMod(200) approximation as observed by comparing the contour plots in Figure 18, left and right.

Finally, to qualitatively assess the performances of the educated HiMod bases, we modify the boundary data assigned on the faces $F_B = (0, 2) \times (0, 1) \times \{z = 0\}$ and $F_T = (1, 2) \times (0, 1) \times \{z = 2\}$, where we enforce now the Robin data $\nabla u \cdot \mathbf{n} + 4u = 0$. We also move the location of the sources S_2 and S_3 by centering them at $(1.1, 0.5, 0.1)$ and $(1.3, 0.5, 1.5)$, respectively. The assignment of the Robin condition and the shift downward of S_2 yields a complex dynamics in the bottom part of the domain and, in particular, on the face F_B, as shown by the contour plot of the reference FE1 approximation in Figure 20, left (transverse section at $y = 0.5$). The computational mesh is reported in Figure 19, left. We preserve the choices made in the previous test case setting for the HiMod reduction and the domain decomposition scheme, except for the use of a modal basis educated with respect to the Robin conditions. In Figure 20, center and right we show the contour plots of the eHiMod(100) and eHiMod(200). As expected, the accuracy of the reduced solution improves by increasing the number of educated modal functions.

We stress again the point that e-HiMod is not intended to provide a new 3D solver, but to give a method for modulating the accuracy for the secondary transverse dynamics, so to be able of covering networks of pipes improving simple 1D models. Nevertheless, this example shows that e-HiMod can work on nontrivial geometries yet approaching the full solution in a "psychologically 1D" framework. An appropriate selection of the modes m can attain the right trade off for working on networks.
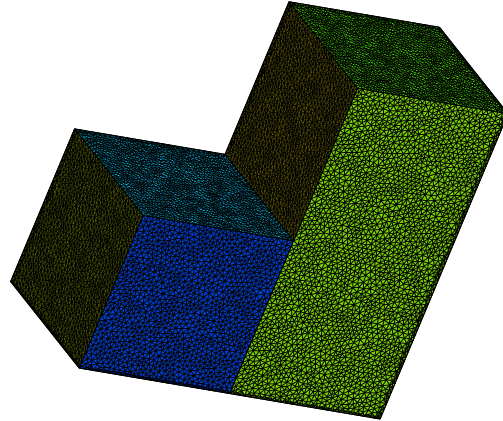
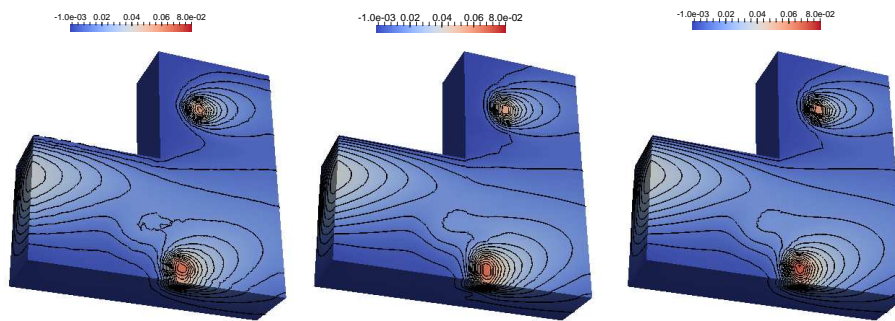Figure 19: Computational mesh for the FE solution of the 3D BFS cases

Figure 20: 3D backward facing step, Dirichlet/Robin BC. Reference FE1 solution (left); HiMod(m) reduced solution for $m = 100$ (left) and $m = 200$ (right).

6 Conclusions

The HiMod procedure follows up the idea of combining separation of variables with a diverse numerical approximation to take advantage from particular features of the problem at hand. For problems with a clear 1D mainstream like fluid dynamics in pipes, the choice of modal approximation for transverse dynamics is quite natural. The framework "1D + transverse components" carries several advantages as for the general structure of the algebraic problems, for the adaptivity and for the efficiency of the solver. Despite of its simplicity, several details need to be understood. In this paper we consider in detail the problem of general boundary conditions on the wall of the pipes. This is crucial in view of practical applications of the method in particular for fluid-structure interaction problems, where the effect of the structure on the fluid can be often represented by Robin boundary conditions on the moving boundaries. We demonstrated that the construction of basis functions based on the solution of SLE problems provides an effective approach for automatically incorporating general boundary conditions with the same performances previously obtained for Dirichlet conditions. Results have been rigorously proved in view of the SLE approximation theory. We also detected some cases that imply superconvergent results, depending of the type of boundary conditions and the regularity of the solution.

We plan to extend this method to more complex problems including incompressible Navier-Stokes equations in both rectilinear and curved cylindrical pipes, to be applied to simplified models of the human circulation. We also intend to exploit in more detail the computational advantages of the 1D-like pattern of the linear system obtained by the e-HiMod procedure. This is expected to even improve the computational advantages of the methodology.

Acknowledgment

References

[1] A. Ern, S. Perotto, and A. Veneziani. *Hierarchical model reduction for advection-diffusion-reaction problems.* In K. Kunisch, Günther O., and O. Steinbach, editors, *Numerical Mathematics and Advanced Applications*. Springer Berlin Heidelberg, 2008.

[2] L. Formaggia, A. Quarteroni, and A. Veneziani, Multiscale models for the Vascular System, in L. Formaggia, A. Quarteroni, A. Veneziani (eds.), Cardiovascular Mathematics, Springer (2009), Chapter 11, pp. 395-446

[3] A. Osiadacz, Simulation and Analysis of Gas Networks, Gulf Publishing Company, Houston, TX, 1987

[4] E. Estrada, The Structure of Complex Networks: Theory and Applications, Oxford University Press, 2011

[5] S. Perotto, A. Zilio, *Space-time adaptive hierarchical model reduction for parabolic equations*, 2015 MOX Report 06/2015, `http://mox.polimi.it`

[6] S. Perotto. *Hierarchical model (Hi-Mod) reduction in non-rectilinear domains*. In Domain Decomposition Methods in Science and Engineering. Series: Lect. Notes Comput. Sci. Eng., Vol. 98, Springer, C. J. Erhel, M. Gander, L. Halpern, G. Pichot, T. Sassi, O. Widlund (eds.) (2014), 477-485.

[7] S. Perotto, A. Ern, and A. Veneziani. *Hierarchical local model reduction for elliptic problems: a domain decomposition approach. Multiscale Model. Simul.*, 8(4):1102–1127, 2010.

[8] Y. Pinchover and J. Rubinstein, An Introduction to Partial Differential Equations, *Cambridge University Press* (2005).

[9] C. Canuto, Y. Hussaini, A. Quarteroni and T.A. Zang, Spectral Methods: Fundamentals in Single Domains. Springer, Berlin, 2006.

[10] C. Canuto, Y. Hussaini, A. Quarteroni and T.A. Zang, Spectral Methods: volution to Complex Geometries and Applications to Fluid Dynamics. Springer, Berlin, 2007.

[11] F. Hecht. *New development in FreeFem++*. J. Numer. Math., 20(3-4):251–265, 2012.

[12] S. Perotto and A. Veneziani. *Coupled model and grid adaptivity in hierarchical reduction of elliptic problems*. J. Sci. Comput., 60(3), 505-536, 2014

[13] M. Vogelius and I. Babuška. *On a dimensional reduction method. I. The optimal selection of basis functions.* Math. Comp., 37(155):31–46, 1981.

[14] M. Vogelius and I. Babuška. *On a dimensional reduction method. II. Some approximation-theoretic results.* Math. Comp., 37(155):47–68, 1981.

[15] M. Vogelius and I. Babuška. *On a dimensional reduction method. III. A posteriori error estimation and an adaptive approach*. Math. Comp., 37(156):361–384, 1981.

[16] C. Canuto, Y. Maday, and A. Quarteroni. *Analysis of the combined finite element and Fourier interpolation.* Numer. Math., 39(2):205–220, 1982.

[17] C. Canuto, Y. Maday, and A. Quarteroni. *Combined finite element and spectral approximation of the Navier-Stokes equations.* Numer. Math., 44(2):201–217, 1984.

[18] A. Ern and J.L. Guermond. Theory and Practice of Finite Elements. Number v. 159 in Applied Mathematical Sciences. Springer, 2004.

[19] J.L. Lions and E. Magenes. Non-homogeneous Boundary Value Problems and Applications. Springer-Verlag, 1972.

[20] S. Perotto and A. Zilio. *Hierarchical model reduction: three different approaches.* In A. Cangiani, R. L. Davidchack, E. Georgoulis, A. N. Gorban, J. Levesley, M. V. Tretyakov, (eds.) *Numerical Mathematics and Advanced Applications 2011.* Springer Berlin Heidelberg, 2013.

[21] M. Aletti, A. Bortolossi, S. Perotto, and A. Veneziani, *One-dimensional surrogate models for advection-diffusion problems*, Numerical Mathematics and Advanced Applications. Series: Lect. Notes Comput. Sci. Eng., Vol. 103, Springer A. Abdulle, S. Deparis, D. Kressner, F. Nobile, M. Picasso (eds.) (2015), 447-456.

[22] `https://cmcsforge.epfl.ch/doxygen/lifev/`.

[23] M. Azaiez, J. Shen, C. Xu, and Q. Zhuang, *A Laguerre-Legendre spectral method for the Stokes problem in a semi-infinite channel* SIAM J Num Anal, 2009, Vol. 47(1) : pp. 271-292

[24] S. Salsa, Partial Differential Equations in Action, Springer, Milan, 2015

[25] L. Zielinski, *Asymptotic distribution of eigenvalues for elliptic boundary value problems*, Asymptotic Analysis 16.3 (1998): 181-201.

[26] L. Landau, *Monotonicity and bounds on Bessel functions*, Mathematical Physics and Quantum Field Theory, Electronic J Diff Eq, Conf. 04, 2000, pp. 147-154

[27] J. Peiró and A. Veneziani, *Reduced models for the Cardiovascular System,* in L. Formaggia, A. Quarteroni, A. Veneziani (eds.), Cardiovascular Mathematics, Springer (2009), Chapter 10, pp. 347-394

MOX Technical Reports, last issues

Dipartimento di Matematica
Politecnico di Milano, Via Bonardi 9 - 20133 Milano (Italy)

36/2015   Fedele, M.; Faggiano, E.; Barbarotta, L.; Cremonesi, F.; Formaggia, L.; Perotto, S.
Semi-Automatic Three-Dimensional Vessel Segmentation Using a Connected Component Localization of the Region-Scalable Fitting Energy

35/2015   Manzoni, A.; Pagani, S.
A certified reduced basis method for PDE-constrained parametric optimization problems by an adjoint-based approach

31/2015   Pini, A.; Vantini, S.; Colombo, D.; Colosimo, B. M.; Previtali, B.
Domain-selective functional ANOVA for process analysis via signal data: the remote monitoring in laser welding

32/2015   Agasisti,T.; Ieva, F.; Masci, C.;Paganoni, A.M.
Does class matter more than school? Evidence from a multilevel statistical analysis on Italian junior secondary school students

33/2015   Fumagalli, A; Pasquale, L; Zonca, S.; Micheletti, S.
An upscaling procedure for fractured reservoirs with non-matching grids

34/2015   Bernardi, M.S.; Mazza, G.; Ramsay, J.O.; Sangalli, L.M.
A separable model for spatial functional data with application to the analysis of the production of waste in Venice province

28/2015   Taffetani, M.; Ciarletta, P.
Beading instability in soft cylindrical gels with capillary energy: weakly non-linear analysis and numerical simulations

30/2015   Pini, A.; Vantini, S.
Interval-wise testing for functional data

29/2015   Antonietti, P.F.; Cangiani, A.; Collis, J.; Dong, Z.; Georgoulis, E.H.; Giani, S.; Houston, P.
Review of Discontinuous Galerkin Finite Element Methods for Partial Differential Equations on Complicated Domains

25/2015   Del Pra, M.; Fumagalli, A.; Scotti, A.
Well posedness of fully coupled fracture/bulk Darcy flow with XFEM